iScience

CellPress
OPEN ACCESS

Article

A feedback loop between plakophilin 4 and YAP signaling regulates keratinocyte differentiation

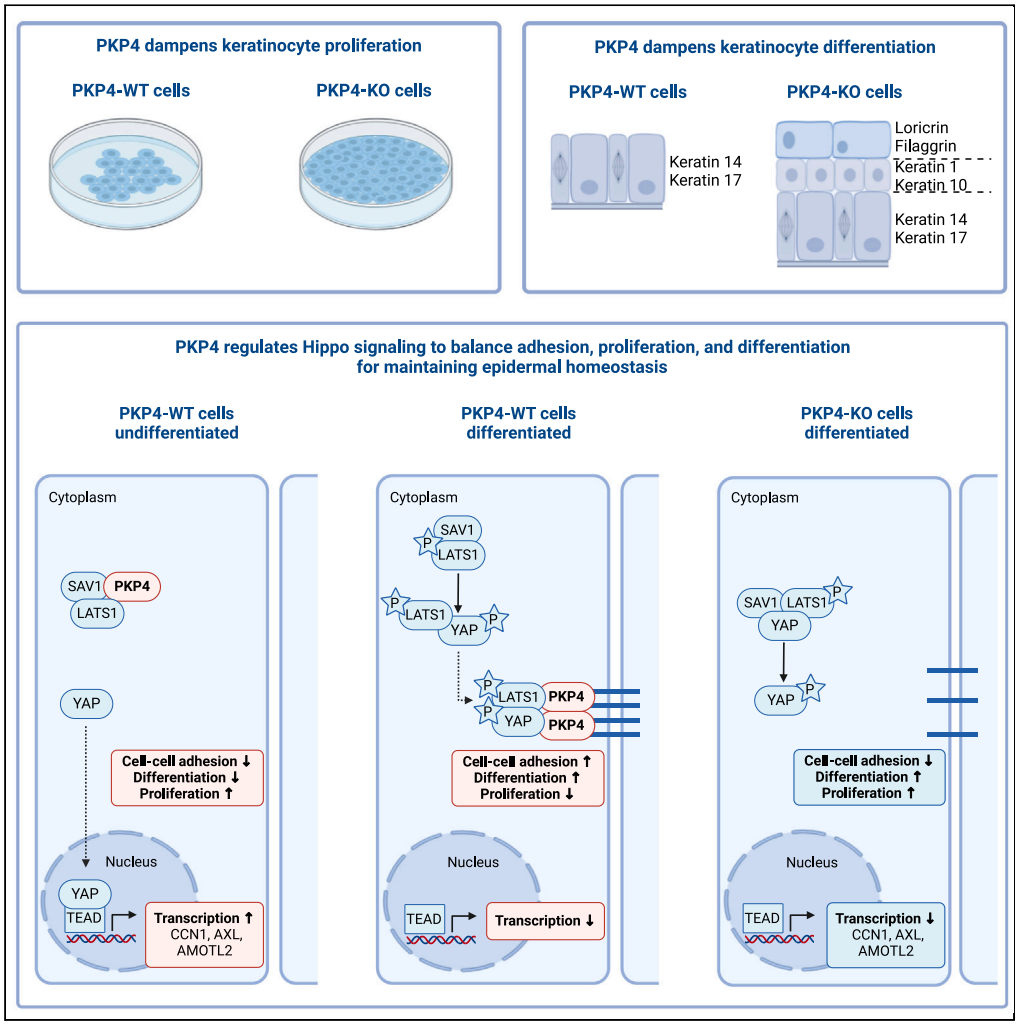

Lisa Müller, Tony Gutschner, Mechthild Hatzfeld

lisa.mueller@uk-halle.de

Highlights

Plakophilin 4 (PKP4) suppresses keratinocyte proliferation

PKP4 prevents premature epidermal differentiation, delamination, and stratification

PKP4 promotes nuclear YAP localization and YAP target gene expression

YAP regulates PKP4 expression through a feedback mechanism

Müller et al., iScience 27, 110762
September 20, 2024
https://doi.org/10.1016/j.isci.2024.110762

iScience

CellPress
OPEN ACCESS

Article

A feedback loop between plakophilin 4 and YAP signaling regulates keratinocyte differentiation

Lisa Müller,[1,2,3,*] Tony Gutschner,[2] and Mechthild Hatzfeld[1]

SUMMARY

The Hippo signaling pathway is an important regulator of organ growth and differentiation, and its deregulation contributes to the development of cancer. The activity of its downstream targets YAP/TAZ depends on adherens junctions. Plakophilin 4 (PKP4) is a cell-type specific adherens junction protein expressed in the proliferating cells of the epidermis. Here, we show that PKP4 diminishes proliferation as well as differentiation. Depletion of PKP4 increased proliferation but at the same time induced premature epidermal differentiation. PKP4 interacted with several Hippo pathway components, including the transcriptional co-activators YAP/TAZ, and promoted nuclear YAP localization and target gene expression. In differentiated keratinocytes, PKP4 recruited LATS and YAP to cell junctions where YAP is transcriptionally inactive. YAP depletion, on the other hand, reduced PKP4 levels and keratinocyte adhesion indicative of a feedback mechanism controlling adhesion, proliferation, and differentiation by balancing YAP functions.

INTRODUCTION

The Hippo pathway is known as a central regulator of cell fate and proliferation. In the skin, the Hippo signaling pathway and its downstream effectors, the transcriptional coactivators Yes-associated protein (YAP) and transcriptional coactivator with PDZ-binding motif (TAZ), control tissue-specific functions during development, homeostasis, and regeneration. When Hippo signaling is inactive, nuclear YAP/TAZ associate with transcriptional enhanced associated domain (TEAD) transcription factors to promote target gene expression.[1,2] Target genes include cell cycle, cell migration, and cell fate regulators. In the epidermis, nuclear localization of YAP/TAZ is essentially restricted to the basal layer, and the extent of cycling activity of epidermal stem cells (SCs) correlated with its nuclear localization.[3] Mice with an epidermis-specific YAP knockout revealed severe epidermal hypoplasia due to insufficient proliferation of SCs, whereas expression of an active mutant YAP (YAP-Ser127Ala) induced thickening of the epidermis resulting from increased proliferation and reduced terminal differentiation supporting a role of YAP in controlling epidermal proliferation.[4]

The Hippo pathway functions as a sensor for tissue and cellular integrity and is modulated in response to mechanical strains and changes in cell-cell and cell-ECM adhesion. Cell junctions appear as major hubs that organize Hippo pathway components.[5] This implies that the Hippo pathway is sensitive to changes in cellular morphology and architecture. Adherens junctions (AJs) can transduce the effects of mechanical stress in an epithelial tissue into the Hippo pathway.[6,7] At a molecular level, α-catenin was found in a tripartite complex with phosphorylated YAP and 14-3-3 in keratinocytes which prevents YAP nuclear localization and inhibits its transcriptional activity.[8,9]

Thus, a connection between the Hippo pathway and AJs is well known. However, it has not been addressed so far if and how the composition of AJs may influence Hippo pathway activity. PKP4 is a component of AJs related to p120-catenin (p120).[10,11] Its expression is restricted to the basal layer of the epidermis[12] whereas the homologous p120 reveals global expression throughout all cell layers.[13] The restricted expression of PKP4 in basal cells implies AJs of different composition depending on the differentiation in the epidermis. PKP4 and p120 share a function in stabilizing classical cadherins at the plasma membrane.[14] However, individual functions have not been characterized so far and the relevance of the differential expression is not clear.[12]

Here, we have analyzed the function of the AJ protein PKP4 in murine keratinocytes. We show that a lack of PKP4 affects keratinocyte proliferation and differentiation. PKP4 promotes the nuclear localization of YAP and YAP target gene expression and prevents premature differentiation whereas a loss of PKP4 promotes differentiation and facilitates delamination of basal cells. In differentiating cells, PKP4 recruits YAP to the plasma membrane to limit its proliferative function. YAP on the other hand appears to stabilize the PKP4 protein which in turn strengthens intercellular adhesion. Thus, we identify a feedback loop between PKP4 and YAP which regulates epidermal homeostasis.

[1]Institute of Molecular Medicine, Section for Pathochemistry, Martin Luther University Halle-Wittenberg, Charles Tanford Protein Research Center, Kurt-Mothes-Str. 3A, 06120 Halle, Germany
[2]Institute of Molecular Medicine, Section for RNA Biology and Pathogenesis, Martin Luther University Halle-Wittenberg, Charles Tanford Protein Research Center, Kurt-Mothes-Str. 3A, 06120 Halle, Germany
[3]Lead contact
*Correspondence: lisa.mueller@uk-halle.de
https://doi.org/10.1016/j.isci.2024.110762

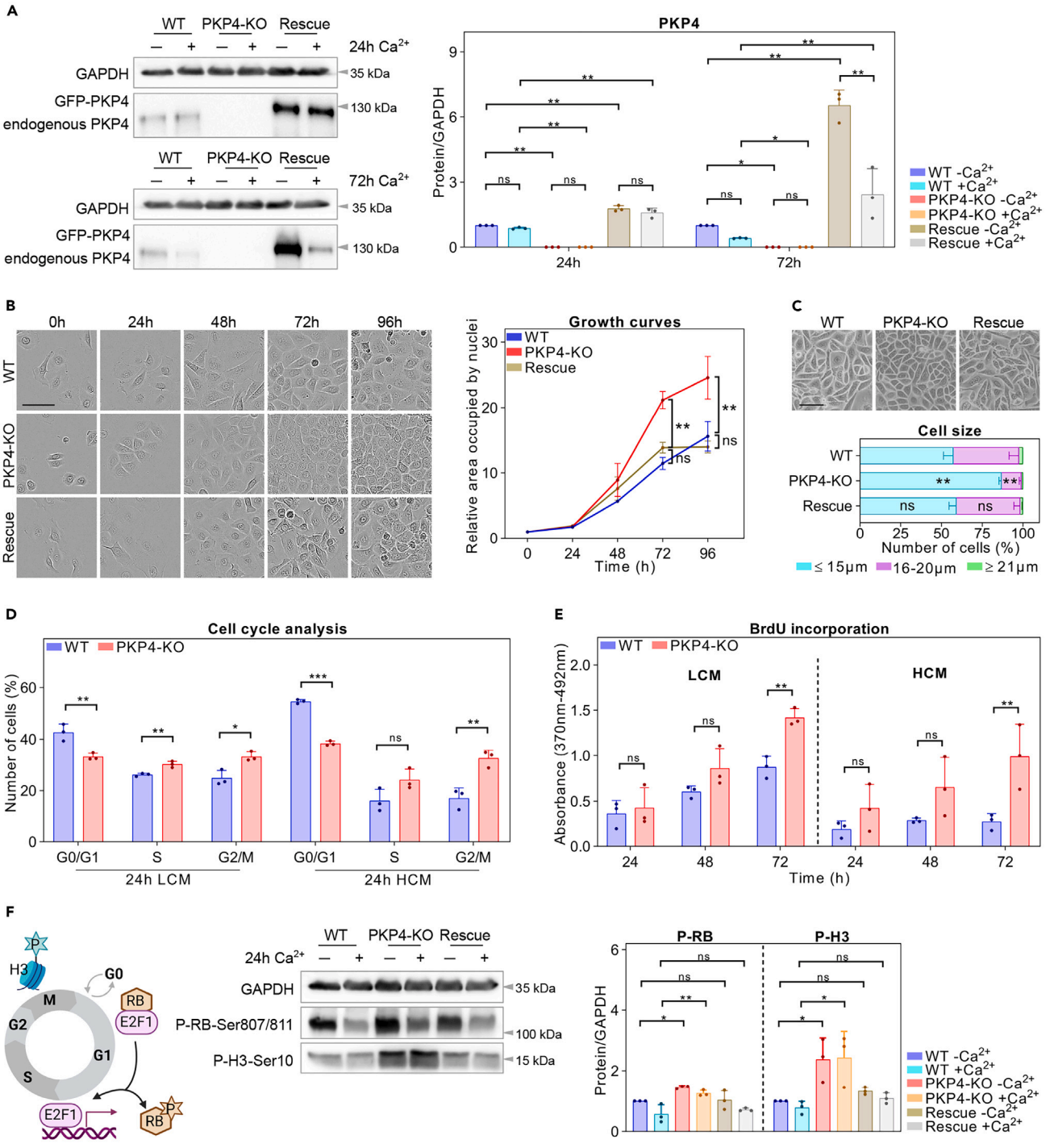

Figure 1. PKP4 modulates keratinocyte proliferation

(A) Levels of PKP4 protein in WT, PKP4-KO, and PKP4-KO+PKP4 (Rescue) cells grown for 24h or 72h in medium with or without Ca^{2+}. Left: Representative western blots of PKP4. GAPDH was used as a loading control. Right: Quantification of PKP4 protein amounts normalized to GAPDH and relative to WT cells grown in medium without Ca^{2+}. Averages +SD from three independent experiments are plotted.

(B) Measurement of proliferation using an IncuCyte S3 system. Left: Representative live cell images of WT, PKP4-KO, and PKP4-KO+PKP4 (Rescue) cells grown for up to 96h in LCM. Scale bar = 100 μm. Right: Area occupied by cell nuclei at the indicated time points, as determined from live cell images. Data are shown relative to measurements at the beginning of recording (time zero). Graphs represent average values from three independent experiments.

Figure 1. *Continued*

(C) The diameter of trypsinized WT, PKP4-KO, and PKP4-KO+PKP4 (Rescue) cells grown for 24h in LCM automatically measured using the BioRad TC20 Cell Counter. Top: Representative live cell images. Scale bar = 100 μm. Bottom: Quantification of cell size. Averages +SD from three independent experiments are plotted. $n \geq 1{,}000$ cells per condition.

(D) Propidium iodide-labeling and flow cytometry analysis of the cell cycle. Number of WT and PKP4-KO cells grown for 24h in LCM or HCM in G0/G1 phase, S phase, or G2/M phase. Averages +SD from three independent experiments are plotted.

(E) BrdU incorporation in WT and PKP4-KO cells grown for 24h, 48h, or 72h in LCM or HCM. Averages +SD from three independent experiments are plotted.

(F) Levels of proliferation markers in WT, PKP4-KO, and PKP4-KO+PKP4 (Rescue) cells grown for 24h in medium with or without Ca^{2+}. Left: Schematic of cell cycle dependent expression of RB and H3. Since RB is phosphorylated in late G1 phase, thereby releasing E2F1 and promoting its transcriptional activity, phospho-RB was used as a marker for G1-S phase transition. Phosphorylation of H3 served as an M phase marker. Mid: Representative western blots of phospho-RB and phospho-H3. GAPDH was used as a loading control. Right: Quantification of phosphorylation levels normalized to GAPDH and relative to WT cells grown in medium without Ca^{2+}. Averages +SD from three independent experiments are plotted. Quantification of LCM versus HCM treatment has been omitted. $*p < 0.05$; $**p < 0.01$; $***p < 0.001$; ns, not significant. Significance was determined by one-way ANOVA with Tukey's multiple comparisons test (A, B, C, and F) or by student's unpaired two-tailed t-test (D and E).

RESULTS

As a model system to study the function of PKP4, we used murine wildtype (WT) keratinocytes, PKP4-knockout (PKP4-KO) keratinocytes, and PKP4-KO keratinocytes overexpressing PKP4-GFP (PKP4-KO+PKP4, Rescue cell line). Since PKP4 expression is restricted to the basal layer of the epidermis[12] and correlates with an undifferentiated cell state, we assumed that treatment of keratinocytes with Ca^{2+} to induce differentiation *in vitro* might decrease the PKP4 protein level. As expected, maintaining the cells in high calcium medium (HCM) for 72h resulted in slightly decreased PKP4 protein level in WT keratinocytes and significantly decreased PKP4 protein levels in Rescue cells (Figure 1A). Since the effect was observed with the GFP-PKP4 construct that lacks any regulatory sequences, we conclude that the decline results primarily from reduced protein stability rather than transcriptional or translational regulation.

PKP4 modulates keratinocyte proliferation

Since epidermal stem cells as well as the transit amplifying cells (TACs) that are both responsible for epidermal regeneration reside in the basal layer, we wondered if PKP4 expression might correlate with the proliferative potential of keratinocytes. To test this assumption, cell proliferation of WT, PKP4-KO, and Rescue keratinocytes maintained in low calcium medium (LCM) was tracked using an IncuCyte S3 system (Figure 1B). As a measure of cell numbers, the area occupied by nuclei was monitored for 4 days. Growth rates differed between WT, PKP4-KO, and Rescue cells. WT and Rescue keratinocytes had similar growth patterns with continuous proliferation. In contrast, loss of PKP4 resulted in an increased growth curve as indicated by a steep ascent of the relative area occupied by nuclei, suggesting that PKP4 limits proliferation in non-transformed keratinocytes.

Since rapidly proliferating cells typically have a reduced size compared to slowly proliferating cells,[15] we automatically measured the diameter of trypsinized WT, PKP4-KO, and Rescue cells maintained in LCM using the BioRad TC20 Cell Counter (Figure 1C). The loss of PKP4 resulted in a significantly increased amounts of small cells, indicating that PKP4 expression correlates with larger cell size and slow proliferation.

To determine more directly which phase of the cell cycle was primarily affected, the proportion of cells in G0/G1, S, and G2 phase/mitosis was measured by flow cytometry. This analysis showed a reduction of PKP4-KO cells in G0/G1 but an enrichment of these cells in S (only in LCM) and G2/mitosis. This decrease of cells in G0/G1 phase and increase of cells in G2/mitosis was independent of Ca^{2+} treatment indicating that the induction of differentiation did not immediately stop proliferation (Figure 1D).

To compare the number of cells in S phase, we measured the incorporation of 5-bromo-2′-desoxyuridine (BrdU) into newly synthesized DNA (Figure 1E). BrdU incorporation was significantly increased in PKP4-KO cells after 72h, even after Ca^{2+} treatment (HCM conditions). This indicates an increase in the number of cells in S phase. This finding correlates with the cell cycle analyses and further supports a rapid proliferation of PKP4-KO keratinocytes.

Western blot analysis of phospho-retinoblastoma protein (P-RB-Ser807/811) as a marker of G1/S-phase transition and phospho-histone H3 (P-H3-Ser10) as marker of mitotic cells confirmed an increase of these markers in PKP4-KO cells, again independent of 24h Ca^{2+} treatment (Figure 1F). This further supports the conclusion that cell cycle progression and thus proliferation was increased in PKP4-KO cells. Taken together, these data indicate that PKP4 limits proliferation by suppressing G1/S phase progression.

PKP4 modulates keratinocyte differentiation

Keratinocytes proliferate in the basal layer of the epidermis but start to differentiate upon stratification. Thus, proliferation and differentiation are typically inversely correlated. However, differentiation and proliferation although regulated simultaneously are independent and cells often start differentiating long before they stop dividing. This allows expansion of cell numbers and acquisition of differentiated function to occur in parallel.[16] When cells stop proliferating, they can irreversible exit the cell cycle and become terminally differentiated or the cells can enter the quiescent phase (G0), from which they can reenter the cell cycle. Quiescence is an important feature of many types of stem cells.[17] The expression of differentiation-specific markers enables quiescence and differentiation of epidermal cells to be distinguished. Keratin 14 and keratin 17 expression is associated with basal epidermal cell characteristics. Early epidermal differentiation is characterized by the expression of keratin 1 and keratin 10 in the spinous layer of the epidermis,[18] whereas involucrin, loricrin, and filaggrin are expressed in the upper corneal and granular layers (Figure S1). To examine whether differentiation was affected in PKP4-KO cells, we analyzed the expression

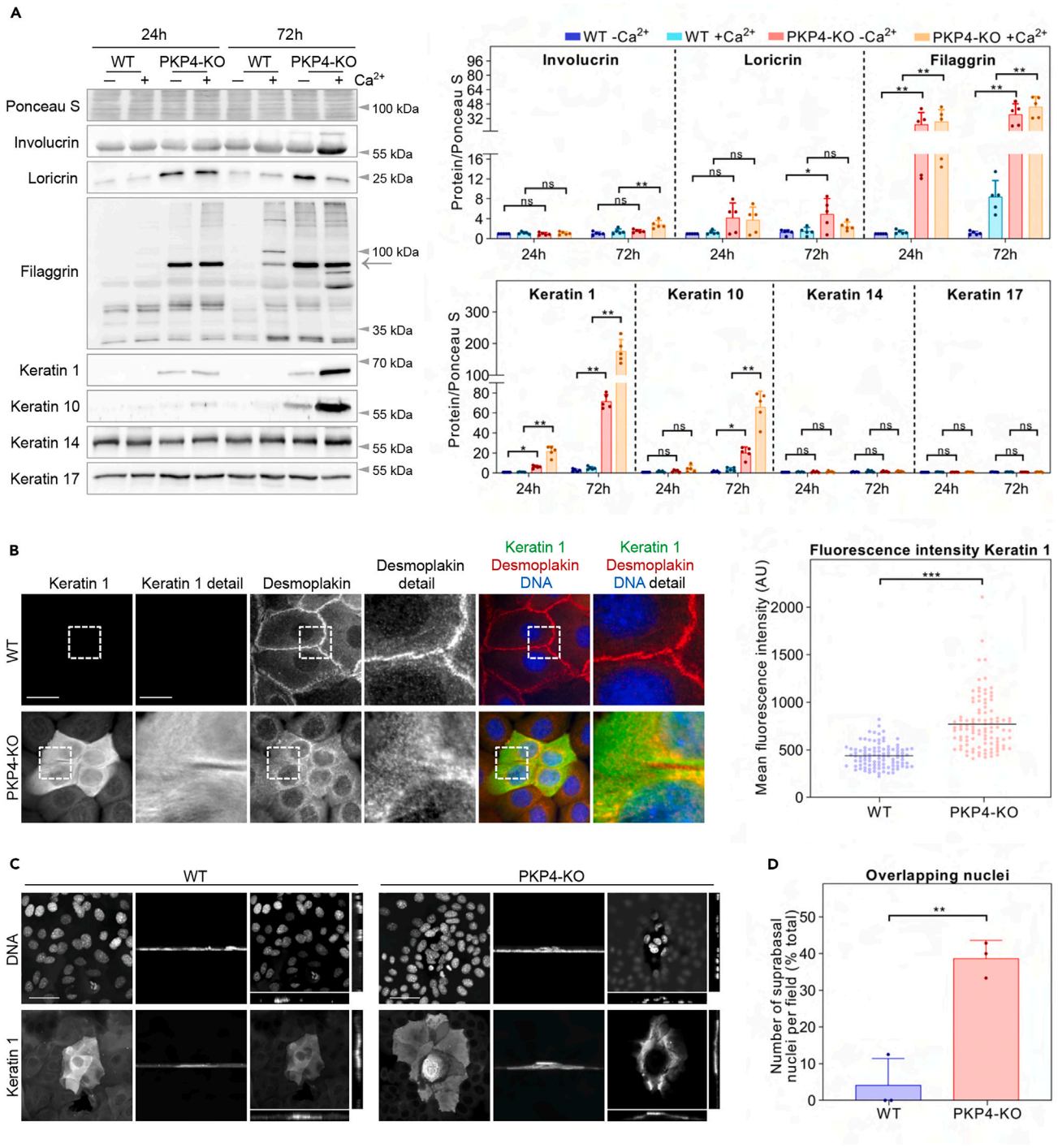

Figure 2. PKP4 modulates keratinocyte differentiation

(A) Protein levels of differentiation markers in WT and PKP4-KO cells grown for 24h or 72h in medium with or without Ca^{2+}. Left: Representative western blots of epidermal differentiation markers. Ponceau S staining was used as a loading control. For filaggrin, the main band representing the filaggrin three-domain intermediate was quantified (marked with an arrow). Right: Quantification of protein amounts normalized to Ponceau S staining and relative to WT cells grown for 24h in medium without Ca^{2+}. Averages +SD from five independent experiments are plotted. Quantification of LCM versus HCM treatment has been omitted. See also Figure S1.

(B) Immunofluorescence analysis of keratin 1 in WT and PKP4-KO cells grown for 24h in HCM. Left: Representative immunofluorescence images showing desmoplakin (DSP) and keratin 1 localization. Scale bar = 50 μm, detail 10 μm. Right: Mean keratin 1 fluorescence intensity. $n \geq 100$ cells per condition from two independent experiments.

Figure 2. *Continued*

(C) Confocal immunofluorescence analysis of keratin 1 in WT and PKP4-KO cells grown for 72h in HCM. Typical example of confocal microscopy z-stacks showing maximum intensity projection (left panel), 3D project x axis rotation (mid panel), and orthogonal views (right panel) of PKP4-KO cells versus WT cells. Scale bar = 100 μm.

(D) Quantification of the amounts of overlapping nuclei in WT or PKP4-KO cells, as determined from confocal images. Averages +SD from three independent experiments are plotted. *$p < 0.05$; **$p < 0.01$; ***$p < 0.001$; ns, not significant. Significance was determined by one-way ANOVA with Tukey's multiple comparisons test (A) or by student's unpaired two-tailed t-test (B and D).

of several differentiation markers (Figure 2A). The induction of differentiation by 24h and 72h Ca^{2+} treatment resulted in increased protein levels of differentiation markers in PKP4-KO cells compared to WT cells. A premature expression of several differentiation markers including loricrin, filaggrin, and keratins 1 and 10 occurred even in the absence of Ca^{2+} supporting a putative role of PKP4 in preventing differentiation in the basal cell layer. Moreover, these data indicate that increased proliferation does not prevent differentiation of PKP4-KO cells supporting an independent regulation of both processes.

In the epidermis, basal keratinocytes delaminate as they move into the suprabasal layers during differentiation. To analyze whether increased differentiation in PKP4-KO cells is linked to delamination, WT and PKP4-KO cells were maintained for 24h in HCM and processed for immunofluorescence (Figure 2B). Desmoplakin staining was used as a marker for cell junctions. Its localization was altered in PKP4-KO cells with an increase in the cytoplasm and punctate staining along the plasma membrane. More importantly, fluorescence intensity of keratin 1 was significantly higher in PKP4-KO cells than in WT cells. Furthermore, PKP4-KO cells showed expression of the suprabasal keratin 1 in small cell clusters that appeared to localize on top of the other cells suggesting that loss of PKP4 facilitates delamination from the basal cell layer. This assumption was validated by confocal images of keratin 1 in WT and PKP4-KO cells maintained in HCM for 72h (Figure 2C). As cells delaminate and form a suprabasal layer, nuclear staining of basal and suprabasal cells can overlap. An increased number of overlapping nuclei was detected in PKP4-KO cells compared to WT cells indicative of a role of PKP4 in preventing delamination (Figure 2D).

Taken together, we show that PKP4 prevents differentiation and delamination and thus stratification in agreement with its localization in the basal layer of the epidermis.

PKP4 affects the Hippo signaling cascade to modulate YAP localization

To unravel how PKP4 regulates proliferation and differentiation, we analyzed RNA sequencing data from WT and PKP4-KO cells grown for 24h in LCM or HCM (published in[19]). Assessment of gene set enrichment analysis (GSEA) of protein coding genes identified differentially regulated biological pathways and molecular functions. Signaling pathways associated with PKP4 were identified using the gene ontology databases[20] (Figure S2A). The upregulated genes in PKP4-KO cells maintained in LCM or HCM were associated with the terms "cell cycle" (including genes such as Ccnd3, Cdkn1c, Cdkn2c, Mad2l2, and Rb1) and "regulation of keratinocyte differentiation" (e.g., Cdsn, Flg, Ivl, Krt1, Krt10, and Lor) indicating a suppressing role of PKP4 in regulating cell proliferation and differentiation. More importantly, the downregulated genes in PKP4-KO cells were associated with "Hippo signaling" (e.g., Tead1-4, Wwtr1) (Figure S2A). These data suggest that PKP4 might regulate the Hippo signaling pathway.

The Hippo pathway is a conserved signaling cascade that regulates cell proliferation and differentiation to control stem/progenitor cell behavior.[21] The Hippo pathway comprises a kinase cascade (Figure 3A) with mammalian ste2-like kinases 1/2 (MST1/2), the adaptor protein salvador homolog 1 (SAV1), large tumor suppressor kinase 1/2 (LATS1/2), mps one binder 1 (MOB1), and the transcriptional coactivator proteins YAP and TAZ. MST1/2 phosphorylate and activate LATS1/2. Accessory proteins, such as SAV1 and MOB1, promote LATS1/2 activation. Activated LATS1/2 phosphorylates YAP/TAZ which leads either to their degradation or a 14-3-3 protein dependent stabilization in the cytoplasm preventing their transcriptional activity. When Hippo signaling is inactive, dephosphorylated, nuclear YAP/TAZ is active and associates with TEAD transcription factors to promote target gene expression.[1,2] Since YAP activity and PKP4 expression are both observed in the basal layer of the epidermis and correlate with proliferation,[3] we hypothesized that PKP4 might play a role in regulating proliferation and differentiation via Hippo signaling.

To analyze a putative role of PKP4 in the Hippo signaling cascade, we quantified the amounts of proteins involved in this pathway by western blotting (Figure 3B). Protein levels of SAV1 and YAP were unaltered in PKP4-KO cells. However, PKP4-KO cells had increased LATS1 but reduced TAZ protein levels, and this was independent of Ca^{2+} treatment and thus independent of AJ formation. Rescue cells had unaltered LATS1 and TAZ levels compared to WT cells. Thus, PKP4 appeared to affect the expression of the Hippo signaling modulators LATS1 and TAZ independent of its localization in the cytoplasm (Ca^{2+} free medium, LCM) or in junctions (Ca^{2+} containing medium, HCM). Reduced TAZ protein level might result from increased degradation since TAZ contains two phosphodegrons which account for its lower stability compared to YAP.[22] More importantly, increased phosphorylation of MST, LATS, and YAP in PKP4-KO compared to WT cells indicated that the Hippo signaling cascade was more active in PKP4-depleted cells.

Since Hippo pathway activity controls the localization of the transcriptional effectors YAP and TAZ, we wondered if YAP/TAZ localization might differ between WT and PKP4-KO cells. Whereas nuclear YAP/TAZ controls the expression of target genes responsible for proliferation and differentiation, cytoplasmic YAP/TAZ is transcriptionally inactive. To analyze the PKP4-dependent localization of endogenous YAP/TAZ, keratinocytes were processed for immunofluorescence (Figure 3C, for validation of antibody specificity see Figure S2B). All cells revealed nuclear and cytoplasmic signals for YAP and TAZ. More importantly, loss of PKP4 decreased the ratio of nuclear to cytoplasmic YAP and TAZ fluorescence, indicating that PKP4 facilitates nuclear YAP/TAZ localization.

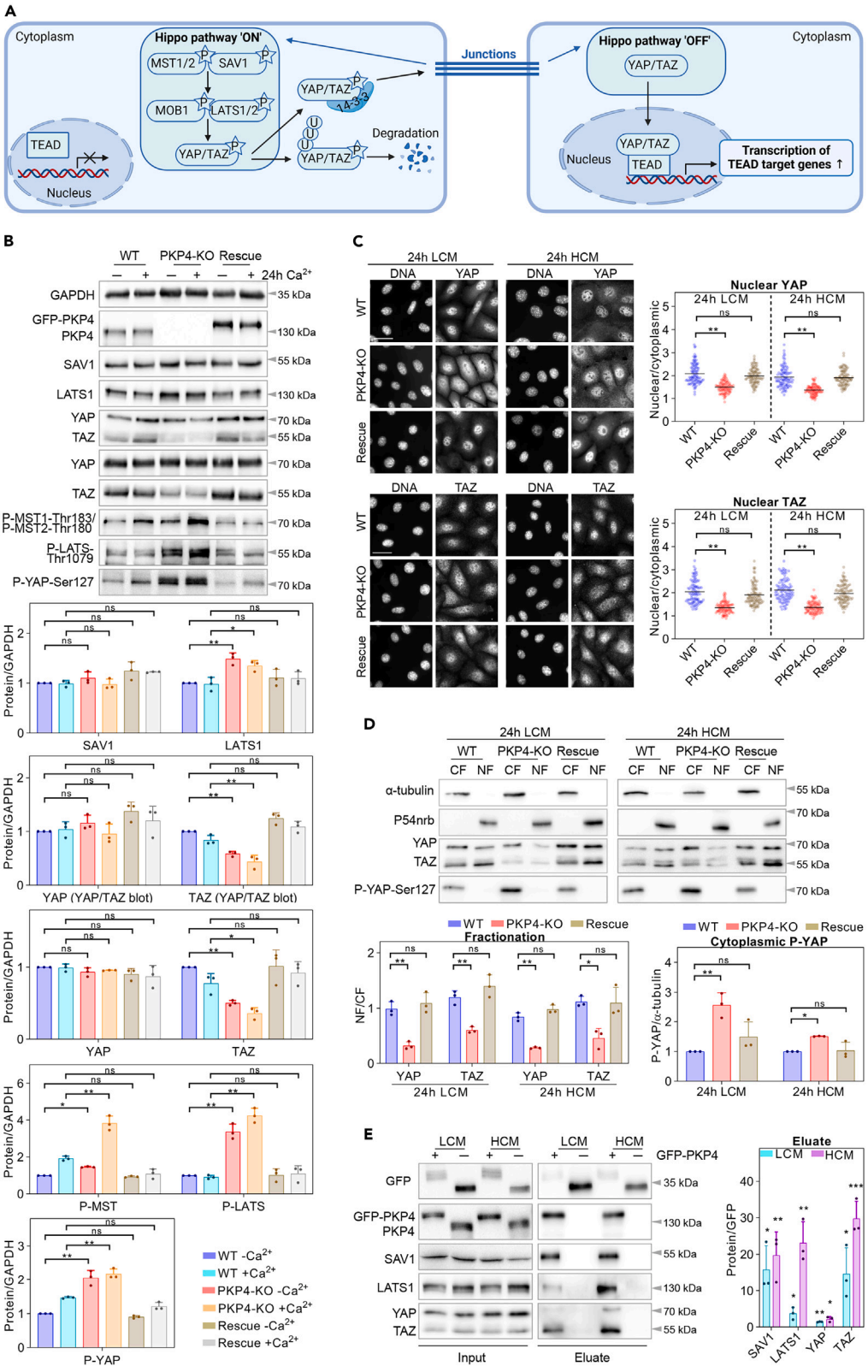
A
Cytoplasm
Hippo pathway 'ON'
MST1/2
SAV1
MOB1
LATS1/2
YAP/TAZ
14-3-3
Degradation
TEAD
Nucleus
Junctions
Hippo pathway 'OFF'
Cytoplasm
YAP/TAZ
Nucleus
YAP/TAZ
TEAD
Transcription of TEAD target genes ↑
B
WT
PKP4-KO
Rescue
24h Ca2+
GAPDH
GFP-PKP4
PKP4
SAV1
LATS1
YAP
TAZ
P-MST1-Thr183/ P-MST2-Thr180
P-LATS-Thr1079
P-YAP-Ser127
35 kDa
130 kDa
55 kDa
70 kDa
Protein/GAPDH
SAV1
LATS1
YAP (YAP/TAZ blot)
TAZ (YAP/TAZ blot)
YAP
TAZ
P-MST
P-LATS
P-YAP
WT -Ca2+
WT +Ca2+
PKP4-KO -Ca2+
PKP4-KO +Ca2+
Rescue -Ca2+
Rescue +Ca2+
C
24h LCM
24h HCM
DNA
YAP
TAZ
WT
PKP4-KO
Rescue
Nuclear YAP
Nuclear TAZ
Nuclear/cytoplasmic
ns
D
CF
NF
α-tubulin
P54nrb
Fractionation
NF/CF
Cytoplasmic P-YAP
P-YAP/α-tubulin
E
LCM
HCM
GFP-PKP4
GFP
Input
Eluate
Protein/GFP

Figure 3. PKP4 affects the Hippo signaling cascade to modulate YAP localization

(A) Schematic of the Hippo signaling pathway. P – phosphorylation. Schematic created with biorender.com.

(B) Protein levels of Hippo signaling modulators in WT, PKP4-KO, and PKP4-KO+PKP4 (Rescue) cells grown for 24h in medium with or without Ca^{2+}. Top: Representative western blots of PKP4 and Hippo signaling modulators. GAPDH was used as a loading control. Bottom: Quantification of protein amounts normalized to GAPDH and relative to WT cells grown in medium without Ca^{2+}. Averages +SD from three independent experiments are plotted. Quantification of LCM versus HCM treatment has been omitted.

(C) Immunofluorescence analysis of YAP (Top) and TAZ (Bottom) localization in WT, PKP4-KO, and PKP4-KO+PKP4 (Rescue) cells grown for 24h in LCM or HCM. Left: Representative immunofluorescence images showing YAP or TAZ localization. Scale bar = 50 μm. Right: Nuclear/cytoplasmic ratio of fluorescence intensities. $n \geq 100$ cells per condition from two independent experiments. See also Figure S2B.

(D) Subcellular fractionation of WT, PKP4-KO, and PKP4-KO+PKP4 (Rescue) cells grown for 24h in LCM or HCM. Top: Representative western blots of cytoplasmic fractions (CF) and nuclear fractions (NF). Bottom left: Quantification of the NF/CF ratio of YAP and TAZ normalized to α-tubulin for CF or P54nrb for NF. Averages +SD from three independent experiments are plotted. Bottom right: Quantification of cytoplasmic P-YAP normalized to α-tubulin and relative to WT cells. Averages +SD from three independent experiments are plotted.

(E) GFP-PKP4 or GFP was affinity-purified from PKP4-KO+PKP4 or WT + GFP cells. Left: Representative western blots of co-purified proteins. Right: Enrichment of SAV1, LATS1, YAP, and TAZ normalized to precipitated GFP and relative to values of GFP cells (second lane in western blot, which was set to 1). Average +SD from three independent experiments are plotted. *$p < 0.05$; **$p < 0.01$; ***$p < 0.001$; ns, not significant. Significance was determined by one-way ANOVA with Tukey's multiple comparisons test (B, C, and D) or by student's unpaired two-tailed t-test (E).

To further validate the PKP4-dependent localization of YAP/TAZ, YAP and TAZ distribution between the cytoplasm and the nucleus was determined after subcellular fractionation of WT, PKP4-KO, and Rescue cells (Figures 3D and S2C). In both LCM and HCM, YAP/TAZ were evenly distributed between cytoplasm and nucleus in WT and Rescue cells. In contrast, PKP4-KO cells showed a highly decreased nuclear YAP/TAZ pool. Thus, the cell fractionation studies support a role of PKP4 in promoting nuclear YAP/TAZ localization. Phosphorylation of YAP interferes with its nuclear localization.[2,23] In agreement, phospho-YAP (P-YAP-Ser127) was exclusively detected in the cytoplasmic fraction of all cells but its level was considerably increased in PKP4-KO cells which was in line with enhanced MST-, LATS-, and YAP phosphorylation (Figure 3B). Thus, PKP4 reduces YAP phosphorylation at Ser127 to facilitate its nuclear import and transcriptional activation. Taken together, these data support a role of PKP4 in turning Hippo signaling down.

To elucidate the molecular mechanism underlying the regulation of Hippo signaling by PKP4, we analyzed whether PKP4 interacts with SAV1, LATS1, YAP, and/or TAZ. GFP-PKP4 was affinity purified from PKP4-KO+PKP4 cells maintained for 24h in LCM or HCM (Figure 3E). SAV1 and LATS1 were co-isolated with PKP4 with increased LATS association in HCM. Moreover, TAZ and to a lesser extent YAP were co-precipitated with PKP4. This indicates an association between PKP4 and Hippo signaling modulators supporting a role of PKP4 in regulating this pathway.

To provide spatial information on where this interaction of PKP4 with LATS and SAV occurs in the cell, PKP4 was co-stained with these Hippo modulators. WT, PKP4-KO, and Rescue cells were maintained for 24h in LCM or HCM and processed for immunofluorescence. After 24h of LCM, SAV localized in the cytoplasm of all cell lines independent of PKP4 expression (Figure S2D). After HCM treatment, PKP4 localized at cell junctions whereas SAV still remained cytoplasmic. In contrast, HCM treatment induced a switch of LATS together with PKP4 from the cytoplasm to cell junctions (Figure S2E). This correlates with the increased PKP4-LATS association in HCM (Figure 3E) where LATS may phosphorylate YAP leading to a reduced nuclear localization of YAP upon keratinocyte differentiation (Figure 3D).

PKP4 promotes YAP target gene expression

Nuclear YAP/TAZ is transcriptionally active increasing the expression of target genes. Since PKP4 affected the nuclear localization of YAP we monitored YAP/TAZ target gene expression in WT, PKP4-KO, and Rescue cells maintained for 24h in LCM or HCM. RNA levels of selected well-known YAP/TAZ-TEAD target transcripts[1] were quantified (Figure 4A). Cellular communication network factor 1 (CCN1, also known as Cyr61), AXL receptor tyrosine kinase (AXL), and angiomotin like 1/2 (AMOTL1/2) mRNAs were downregulated in PKP4-KO cells but unaltered in Rescue cells compared to WT cells. Cellular communication network factor 2 (CCN2, also known as CTGF) and Thrombospondin-1 (THBS1) were also downregulated but re-expression of PKP4 led only to a partial rescue of these transcripts. Taken together, we conclude that PKP4 can regulate YAP/TAZ-TEAD target gene expression.

To validate if *CCN1, AXL, AMOTL1*, and *AMOTL2* were targets of YAP and/or TAZ in keratinocytes, WT cells treated with control (siCtrl), YAP-directed (siYAP), or TAZ-directed (siTAZ) siRNAs were maintained in LCM or HCM and processed for qRT-PCR (Figure 4B). YAP depletion decreased mRNA levels of *CCN1, AXL*, and *AMOTL2*, suggesting that YAP was a positive regulator of these target genes whereas YAP negatively regulated the *TAZ* mRNA level. In contrast, TAZ did not affect the expression of the analyzed genes underscoring a primary role of YAP in controlling the expression of these target genes. These data are in line with our findings that PKP4 suppresses YAP phosphorylation thereby promoting nuclear YAP localization (Figure 3D) and target gene expression (Figure 4A). We conclude that PKP4 facilitates YAP nuclear localization and transcriptional activity to regulate TEAD target gene expression.

YAP affects proliferation and differentiation of keratinocytes

The delicate balance of unphosphorylated to phosphorylated YAP/TAZ determines not only its nuclear localization but through their function as transcriptional co-activators also control cell fate including proliferation and differentiation.[24] To directly link PKP4's role in Hippo signaling with keratinocyte proliferation and differentiation, we analyzed the role of YAP/TAZ in keratinocyte proliferation. WT, PKP4-KO, and Rescue

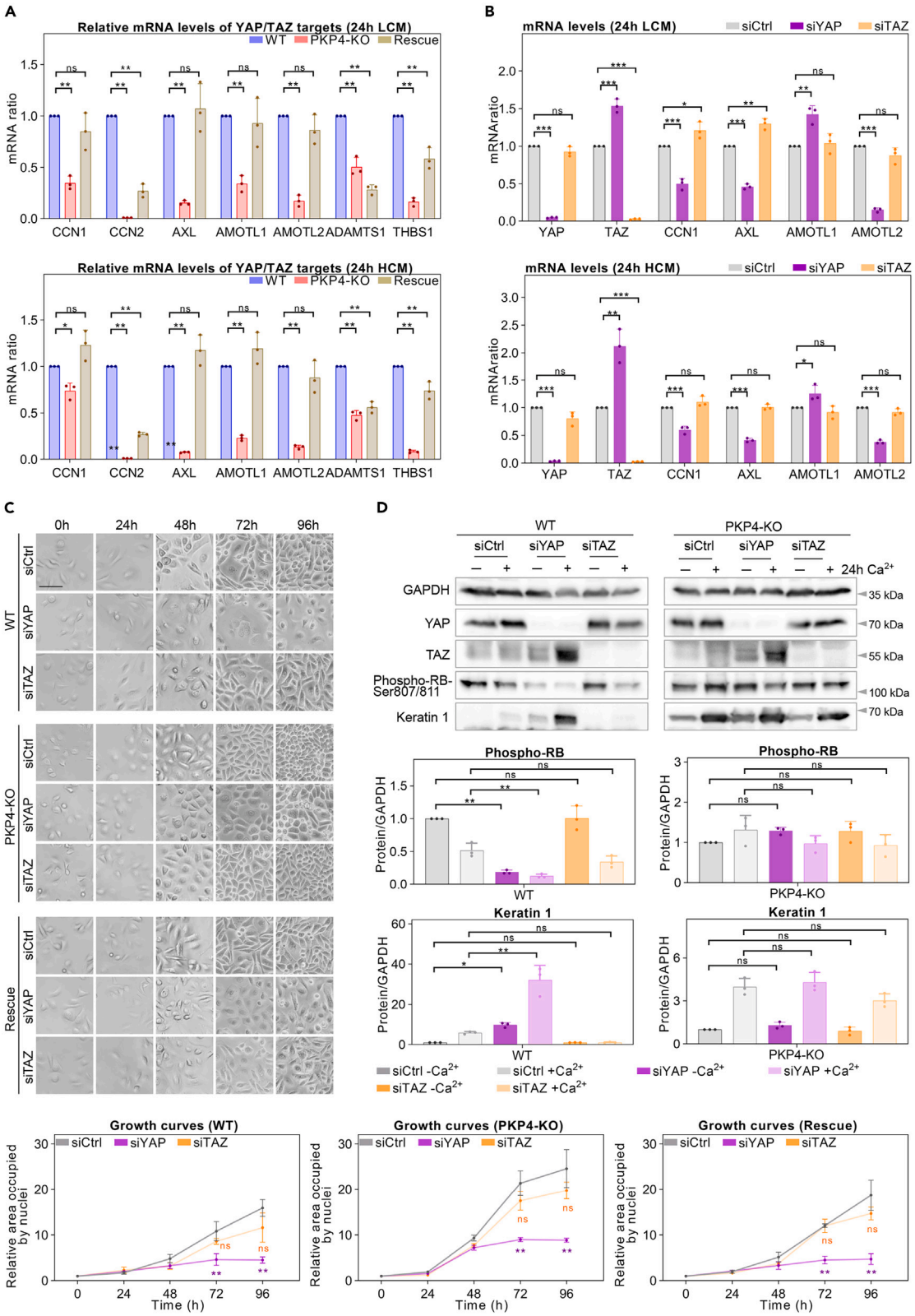
A
Relative mRNA levels of YAP/TAZ targets (24h LCM)
WT PKP4-KO Rescue
mRNA ratio
CCN1 CCN2 AXL AMOTL1 AMOTL2 ADAMTS1 THBS1
Relative mRNA levels of YAP/TAZ targets (24h HCM)
B
mRNA levels (24h LCM)
siCtrl siYAP siTAZ
mRNAratio
YAP TAZ CCN1 AXL AMOTL1 AMOTL2
mRNA levels (24h HCM)
C
0h 24h 48h 72h 96h
WT
PKP4-KO
Rescue
siCtrl
siYAP
siTAZ
D
WT
PKP4-KO
24h Ca2+
GAPDH
YAP
TAZ
Phospho-RB-Ser807/811
Keratin 1
35 kDa
70 kDa
55 kDa
100 kDa
Phospho-RB
Protein/GAPDH
Keratin 1
siCtrl -Ca2+
siCtrl +Ca2+
siYAP -Ca2+
siYAP +Ca2+
siTAZ -Ca2+
siTAZ +Ca2+
Growth curves (WT)
Growth curves (PKP4-KO)
Growth curves (Rescue)
Relative area occupied by nuclei
Time (h)

Figure 4. PKP4 promotes YAP target gene expression and YAP affects proliferation and differentiation of keratinocytes

(A) mRNA amounts of YAP/TAZ targets in PKP4-KO and PKP4-KO+PKP4 (Rescue) cells relative to WT cells grown for 24h in LCM (Top) or HCM (Bottom). *Eif3k* was used as a reference gene. Averages +SD from three independent experiments are plotted.

(B) mRNA amounts of YAP/TAZ targets in siRNA-treated WT cells grown for 24h in LCM (Top) or HCM (Bottom). *Eif3k* was used as a reference gene. Averages +SD from three independent experiments are plotted.

(C) Measurement of proliferation using an IncuCyte S3 system. Top: Representative live cell images of WT, PKP4-KO, and PKP4-KO+PKP4 (Rescue) cells treated with control, YAP- or TAZ directed siRNAs grown for up to 96h in LCM. Scale bar = 100 μm. Bottom: Area occupied by cell nuclei at the indicated time points, as determined from live cell images. Data are shown relative to measurements at the beginning of recording (time zero). Graphs represent averages ±SD from three independent experiments. See also Figure S3A.

(D) Western Blots showing proliferation and differentiation marker expression in siRNA-treated WT and PKP4-KO cells grown for 24h in medium with or without Ca^{2+}. Top: Representative western blots of YAP, TAZ, the proliferation marker phospho-RB, and the differentiation marker keratin 1. GAPDH was used as a loading control. Bottom: Quantification of protein amounts normalized to GAPDH and relative to WT cells grown in medium without Ca^{2+}. Quantification of LCM versus HCM treatment has been omitted. Averages +SD from three independent experiments are plotted. See also Figure S3B. *$p < 0.05$; **$p < 0.01$; ***$p < 0.001$; ns, not significant. Significance was determined by one-way ANOVA with Tukey's multiple comparisons test (A, B, C, and D).

cells were treated with control (siCtrl), YAP-directed (siYAP), or TAZ-directed (siTAZ) siRNAs, and maintained in medium without Ca^{2+} for 96h. Proliferation was tracked using an Incucyte S3 system (Figure 4C, for validation of knockdown efficiencies see Figure S3A). Growth was suppressed in both, WT and Rescue cells, after YAP but not after TAZ depletion. Proliferation was also suppressed in PKP4-KO cells after YAP but not after TAZ knockdown but proliferation remained at an elevated level after YAP depletion.

To validate the effect of YAP on proliferation, the level of phospho-RB as a marker of proliferation was determined by Western Blotting of cell lysates. In WT cells, phospho-RB levels were reduced after YAP depletion in agreement with YAP's role in promoting proliferation (Figure 4D, for validation of knockdown efficiencies see Figure S3B). However, a YAP knockdown in PKP4-KO cells did not significantly reduce the elevated phospho-RB levels in line with the still elevated proliferation of these cells (Figures 4C and 4D). In conclusion, PKP4- and YAP depletion have opposing effects on proliferation and PKP4-dependent attenuation of proliferation might also depend on other pathways that may or may not interact with Hippo signaling.

To analyze whether PKP4-dependent regulation of differentiation might be mediated by its role in Hippo signaling, we analyzed the effect of YAP/TAZ on keratinocyte differentiation. SiRNA-mediated loss of YAP increased the level of the differentiation marker keratin 1 in WT but not in PKP4-KO cells, where keratin 1 expression was already strongly elevated compared to WT cells (Figure 4D). This result suggests that the inactivation of YAP in PKP4-KO cells contributes to the increased expression of keratin 1 in these cells. Thus, YAP and PKP4 might collaborate to suppress the expression of keratin 1 and differentiation. The low increase of keratin 1 in YAP depleted WT cells in LCM conditions but more importantly the high increase in HCM conditions suggests an additional contribution of calcium regulated signaling pathways which comprise a complex network of outside-in as well as inside-out signaling events. YAP depletion also increased TAZ levels in WT and PKP4-KO cells, suggesting that YAP is a negative regulator of TAZ in murine keratinocytes. TAZ depletion, however, did not affect the levels of phospho-RB or keratin 1.

Taken together, we show that PKP4 regulates the Hippo pathway by promoting YAP nuclear localization and its function as a transcriptional co-activator of TEAD transcription factors. YAP depletion downregulated proliferation in WT cells whereas phospho-RB levels and proliferation remained elevated in PKP4-KO cells suggesting additional pathways involved in PKP4-mediated proliferation control. Importantly, depletion of YAP promoted keratin1 expression in WT but not in PKP4-KO cells suggesting that premature differentiation of these cells might depend on Hippo pathway activation.

PKP4 recruits YAP/TAZ to regulate cell-cell adhesion

Since phosphorylated and 14-3-3 bound YAP/TAZ can associate with the junctional complex to keep YAP/TAZ inactive, we asked whether PKP4 might recruit YAP/TAZ to the junctional zone and whether this might have an impact on cell-cell adhesion.

To analyze the junctional localization of endogenous YAP/TAZ in WT, PKP4-KO, and Rescue cells, keratinocytes were maintained in LCM or HCM and processed for immunofluorescence (Figure 5A, for TAZ immunostaining see Figure S4A). In LCM, both PKP4 and YAP/TAZ localized in the cytoplasm and the nucleus. As expected, HCM induced a junctional association of PKP4 in WT cells (Figures 5A and S4A, for quantification see Figure S4B). More importantly, association of YAP and TAZ with lateral membranes increased in WT and Rescue cells maintained in HCM whereas the loss of PKP4 prevented the lateral localization of YAP/TAZ (Figures 5A and S4A). Since YAP/TAZ were only detectable at lateral membranes in WT and Rescue cells maintained in HCM and the association of YAP/TAZ with PKP4 increased in HCM (Figure 3E), we assume that junctional PKP4 facilitates YAP/TAZ association with lateral membranes. Since PKP4 recruited LATS to the membrane (Figure S2E) and the association was enhanced in HCM (Figure 3E), PKP4 may facilitate LATS dependent phosphorylation of cytoplasmic YAP after induction of differentiation to keep YAP inactive and limit proliferation once the differentiation program has been initiated.

To analyze a temporal regulation of YAP localization by PKP4, WT, PKP4-KO, and Rescue cells were maintained in HCM for 72h and processed for immunofluorescence (Figure S4C). After 72h of HCM treatment, YAP localization shifted to the junctional zone in WT and Rescue cells but not in PKP4-KO cells. The increased and more defined junctional association of YAP after 72h of HCM (Figure S4C) compared to 24h of HCM treatment (Figure 5A) suggests that besides the presence of PKP4, junctional maturation facilitated YAP association.

To analyze the requirements for YAP's junction association in more detail, we performed a time course analysis of junction assembly in WT, PKP4-KO, and Rescue cells. Immunostaining of PKP4 and YAP was performed in WT, PKP4-KO, and Rescue cells maintained in HCM for 0h,

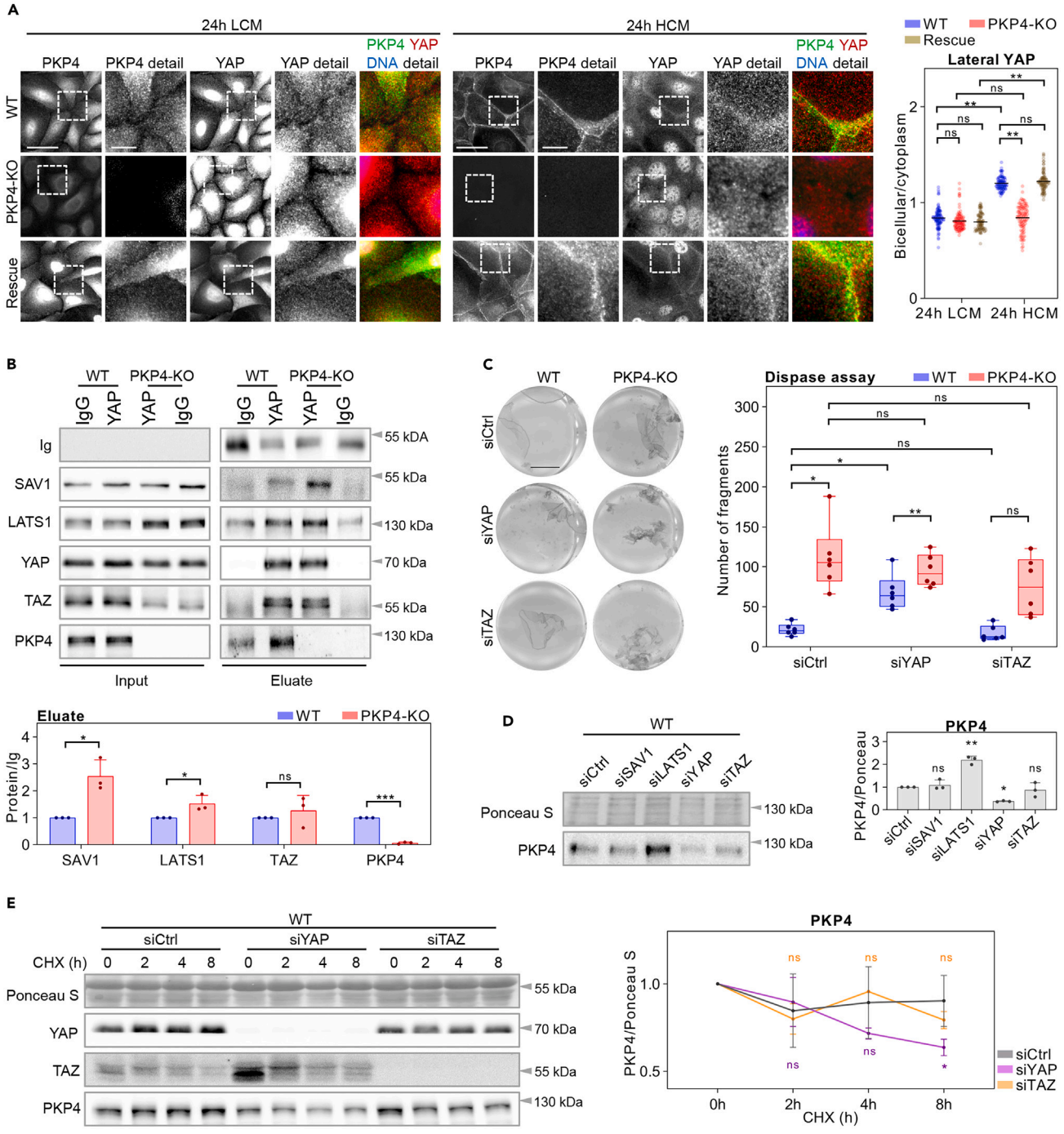

Figure 5. PKP4 recruits YAP/TAZ to regulate cell-cell adhesion

(A) Immunofluorescence analysis of YAP in WT, PKP4-KO, and PKP4-KO+PKP4 (Rescue) cells grown for 24h in LCM or HCM. Left: Representative immunofluorescence images showing PKP4 and YAP localization. Scale bar = 50 μm, detail = 10 μm. Right: Bicellular/cytoplasm ratio of fluorescence intensities. $n \geq 100$ cells per condition from two independent experiments. See also Figure S4B.

(B) Endogenous YAP was affinity-purified from WT and PKP4-KO cells. Top: Representative western blots of co-purifying proteins. Normal rabbit IgG served as negative control. Bottom: Quantification of eluate protein levels normalized to IgG heavy chain and relative to values in WT cells. Averages +SD from three independent experiments are plotted.

(C) Dispase-based dissociation assay of siRNA-treated WT and PKP4-KO cells grown for 24h in HCM. Left: Representative images showing the results of dispase assays after mechanical stress. Scale bar = 5 mm. Right: Quantification of fragment numbers. Boxplots show fragment numbers from six independent experiments. The whiskers extend to the minimum and the maximum values.

Figure 5. *Continued*

(D) PKP4 protein level in *Sav1*, *Lats1*, *Yap* or *Taz* siRNA-treated WT cells grown for 24h in HCM. Left: Representative western blot of PKP4. Ponceau S staining was used as a loading control. Right: Quantification of PKP4 amounts normalized to Ponceau S and relative to siCtrl-treated WT cells. Averages +SD from three independent experiments are plotted. See also Figure S4F.

(E) PKP4 protein stability after CHX treatment in siRNA-treated WT cells grown for 24h in HCM. Left: Representative western blots of YAP, TAZ, and PKP4. Ponceau S staining was used as a loading control. Right: Quantification of PKP4 amounts normalized to Ponceau S. Averages +SD from three independent experiments are plotted. *$p < 0.05$; **$p < 0.01$; ***$p < 0.001$; ns, not significant. Significance was determined by one-way ANOVA with Tukey's multiple comparisons test (A, C, D, and E) or by student's unpaired two-tailed t-test (B).

0.5h, 2h, 4h, or 8h (Figure S4D). HCM rapidly induced PKP4 localization at lateral cell membranes in WT and Rescue cells as indicated by junctional PKP4 localization after 2h HCM treatment. However, even after 8h HCM, YAP did not localize at lateral membranes indicating that the two proteins are not co-transported to the membrane. Moreover, the late association of YAP with the membrane suggests that mature cell junctions are necessary for incorporation of YAP at lateral junctions (Figure 5A).

To further analyze the association of YAP/TAZ with junctions, endogenous YAP (Figure 5B) or TAZ (Figure S4E) was affinity purified from WT and PKP4-KO cells maintained in HCM and probed for interacting proteins by western blotting. PKP4 was co-precipitated by YAP and TAZ from WT cells confirming an association as shown in Figure 3E. In agreement with previous reports, YAP and TAZ co-purified with SAV1 and LATS1. Importantly, this association was increased in PKP4-KO cells compared to WT cells suggesting that PKP4 reduces the stability of this complex to prevent YAP/TAZ phosphorylation resulting in its nuclear localization.

To functionally link YAP/TAZ with cell-cell adhesion, WT and PKP4-KO cells treated with control (siCtrl), YAP-directed (siYAP), or TAZ-directed (siTAZ) siRNAs were maintained in HCM and processed for epithelial sheet assays (Figure 5C). siCtrl treated PKP4-KO cells revealed already increased numbers of fragments compared to WT cells. YAP but not TAZ depletion resulted in an increased number of fragments generated by mechanical stress in WT cells. This suggests that YAP promotes cell-cell adhesion in WT cells. However, YAP or TAZ depletion did not affect the number of fragments in PKP4-KO cells. Therefore, we conclude that the effect of YAP on cell-cell adhesion depended on PKP4.

Since YAP affected keratinocyte differentiation via PKP4 and also promoted intercellular adhesion, we investigated a putative feedback loop between YAP and PKP4. WT cells treated with control (siCtrl), SAV1-directed (siSAV1), LATS1-directed (siLATS1), YAP-directed (siYAP), or TAZ-directed (siTAZ) siRNAs were maintained in HCM and processed for western blotting (Figure 5D, for validation of knockdown efficiencies see Figure S4F). PKP4 protein level was not affected by SAV1 or TAZ knockdown. More importantly, LATS1 depletion increased whereas YAP depletion decreased the PKP4 protein level. This suggests that YAP is a positive regulator of PKP4 protein level.

To analyze whether PKP4 is a transcriptional target of YAP, WT cells treated with control (siCtrl), YAP-directed (siYAP), or TAZ-directed (siTAZ) siRNAs were maintained in HCM and processed for qRT-PCR (Figure S4G). The PKP4 mRNA level was not affected by YAP or TAZ depletion indicating that PKP4 is not a direct transcriptional target of YAP in keratinocytes.

This suggested a regulation at the level of protein stability. To test this assumption, WT cells transfected with control (siCtrl), YAP-directed (siYAP), or TAZ-directed (siTAZ) siRNAs were maintained in HCM, treated with cycloheximide (CHX), and processed for western blotting (Figure 5E). TAZ knockdown had no significant effect on PKP4 protein abundance even after prolonged CHX treatment. In contrast, YAP depletion decreased PKP4 protein stability upon exposure to CHX indicating that YAP prevented PKP4's degradation.

In summary, junctional PKP4 appears to increase YAP association with lateral membranes. YAP in turn seems to stabilize PKP4 at junctions thereby promoting cell-cell adhesion.

DISCUSSION

AJs are key regulators of tissue architecture and dynamics as they control cell proliferation and differentiation. Recent studies have shown that AJs regulate the Hippo pathway and its downstream targets YAP/TAZ to control proliferation and differentiation.[25] However, it is unclear if and how the composition of AJs influences YAP/TAZ regulation and function. Here, we have identified a role of the AJ associated protein PKP4 in attenuating proliferation and differentiation in murine keratinocytes. PKP4 suppressed LATS1 and YAP phosphorylation but also recruited both, LATS1 and YAP, to the cell membrane which leaves YAP transcriptionally inactive. In undifferentiated cells, PKP4 promoted the nuclear localization of YAP and YAP target gene expression. Upon commitment to differentiation, PKP4 recruited LATS1 and YAP to the junctional zone. This suggests that PKP4 affects Hippo signaling pathway activation via a PKP4-LATS1-YAP/TAZ axis. These data imply a role of PKP4 in balancing YAP-dependent proliferation with YAP-dependent junctional stabilization to regulate proliferation in basal cells and in transit-amplifying cells. In basal epidermal keratinocytes, PKP4 might fine-tune YAP activity to prevent hyperproliferation and thus maintain epidermal thickness. The modulation of YAP's subcellular localization by PKP4 identifies PKP4 as a so far unknown regulator of Hippo signaling (summarized in Figure 6).

PKP4 suppresses proliferation and differentiation

Non-cancerous cells stop growth when cell density is too high, a process called "contact inhibition of proliferation" (CIP). This process directly links cell-cell adhesion to proliferation.[26] In most epithelial cells, high cell density or confluence lead to a proliferation arrest and these cells enter a state of quiescence or terminal differentiation. CIP is overcome in embryonic development or wound healing when rapid cell growth and proliferation is required. In contrast, pathological loss of CIP results in uncontrolled proliferation and increases the cell's ability to undergo

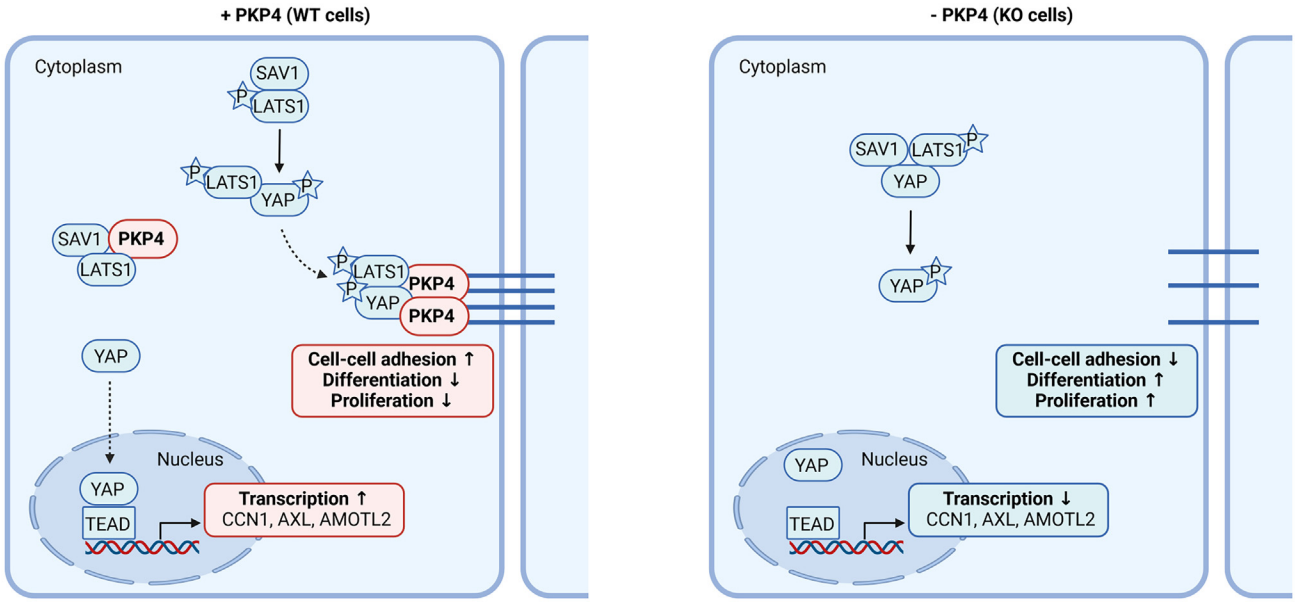

Figure 6. Schematic depicting the putative role of PKP4 in regulating adhesion, proliferation, and differentiation via YAP signaling P – phosphorylation
Schematic created with biorender.com.

malignant transformation. AJs modulate CIP and cell proliferation by promoting growth factor dependence. Depletion of α-catenin e.g., enhanced cell proliferation and decreased the dependence on exogenous growth factors by perturbing AJs.[27] Similarly, conditional targeting of p120 in murine skin induced hyperproliferation and progressive development of skin neoplasias which was associated with intrinsic NF-κB activation.[28,29] We show that the loss of the related protein PKP4 also increased proliferation of murine keratinocytes suggesting that PKP4 acts to maintain CIP. Although only a few studies have addressed PKP4's function in cancer, it has been shown that low levels of PKP4 increased the motility of bladder cancer cells, which might favor aggressive, metastatic tumor progression.[30]

How PKP4's role in repressing proliferation correlates with its expression in the basal layer of the epidermis that includes the stem cell compartment remains incompletely understood. PKP4 reduced not only proliferation but also prevented differentiation, delamination and thus stratification. This correlates with the loss of PKP4 expression in suprabasal cells that undergo differentiation. Earlier studies suggested that proliferation leads to local crowding that drives delamination implicating that proliferation proceeds differentiation.[31,32] However, cell division in the adult seems to occur downstream of basal cell differentiation.[33] Before giving rise to fully differentiated cells, stem cells change to a proliferative state, known as TACs. TACs represent a cell population in transition between stem cells and differentiated cells.[34,35] The simultaneous increase in proliferation and differentiation observed in the PKP4-KO keratinocytes might therefore result from the induction of keratinocyte differentiation followed by transition into TACs to promote self-renewal.

Mutual regulation of PKP4 and YAP activity

Epidermal growth must be carefully balanced: Inadequate proliferation results either in epidermal thinning that perturbs epidermal barrier function, or leads to hyperproliferative disorders caused by excessive growth. The transcriptional coactivators of the Hippo pathway, YAP and TAZ, are crucially involved in the control of cell proliferation and differentiation which regulates the size of organs and tissues. In the suprabasal cells of the adult interfollicular epidermis, YAP was primarily cytoplasmic whereas in basal cells YAP localized primarily in the nucleus, although there is some ambiguity concerning the extent of nuclear YAP in the basal layer.[4,36,37] In support of a role of YAP in promoting keratinocyte proliferation, a conditional knockout of YAP in mouse skin caused epidermal hypoplasia due to insufficient proliferation[8] whereas the expression of a constitutive active YAP mutant (YAP-Ser127Ala) induced epidermal hyperthickening and impaired differentiation.[4,8] Among the regulators of the Hippo pathway are AJs. While p120 seems not to be involved in regulating Hippo signaling,[7] α-catenin binds to 14-3-3 proteins thereby promoting the cytoplasmic retention of YAP which prevents YAP activity in the nucleus and dampens YAP transcriptional activity and proliferation.[8] A skin-specific deletion of *α-catenin* caused keratinocyte hyperproliferation and squamous cell carcinoma that resembled the phenotype observed in YAP overexpressing mice. We observed a similar role for PKP4 which, like α-catenin, reduced keratinocyte proliferation.

Several molecular mechanisms can contribute to PKP4's role in balancing proliferation and differentiation. First, the loss of PKP4 disturbed AJ morphology and prevented tissue tension[19] which interferes with CIP and thus promotes proliferation probably involving mechanosignaling via the cytoskeleton. Second, PKP4 may modulate YAP/TAZ function by interacting with several components of the Hippo pathway. YAP/TAZ bind to gene enhancer elements in complex with TEAD transcription factors, and interact with chromatin remodeling factors to drive or

repress target gene expression.[38–40] YAP/TAZ-TEAD target gens include e.g., *Ccn1, Ccn2, Axl, Amotl* that were downregulated by the loss of PKP4 indicating a role of PKP4 in the regulation of these genes through its interaction with Hippo pathway components and in controlling YAP/TAZ subcellular localization. However, YAP/TAZ functions have also been linked to other pathways such as the Polycomb repressive complex. Polycomb proteins are master regulators that control the balance between proliferation and differentiation. When cells switch to terminal differentiation, the transcription machinery drives the expression of differentiation genes, in part by removing the Polycomb transcriptional repressor complex. Polycomb comprises two protein complexes, Polycomb repressive complex 1 (PRC1) and PRC2. In the developing epidermis, disruption of either PRC1 or PRC2 resulted in the increased expression of a set of target genes[41] whereas the removal of both PRC1 and PRC2 provoked severe morphological defects.[42–44] A LATS2 knockout caused downregulation of PRC2 and H3K27me3. LATS2 promoted PRC2 histone methyltransferase activity and the expression of PRC2 components,[45] thereby preventing premature differentiation. YAP also co-localized with EZH2, the catalytically active subunit of PRC2, on the genome to repress transcription emphasizing an underappreciated aspect of YAP in transcriptional repression.[46]

Well known mammalian target genes silenced by Polycomb proteins include the *Hox* gene clusters.[47] YAP regulated the expression of Hoxa1 and Hoxc13 in oral and dental epithelia as well as in the epidermis[48] again supporting a link between YAP and Polycomb regulatory mechanisms. RNA-sequencing data from WT, PKP4-KO, and Rescue cells[19] revealed an upregulation of the *Hox* gene cluster upon loss of PKP4 suggesting a de-repression in the absence of PKP4 (Figure S5A) and supporting a role of YAP and Polycomb downstream of PKP4. In line with the de-repression of Polycomb target genes, PKP4 knockout cells revealed reduced expression of several Polycomb group proteins including *Bmi1* and *Cbx* genes (Figure S5B).

Additional pathways are involved in regulating YAP/TAZ signaling adding to the complexity of its regulation. This includes factors that modulate YAP/TAZ binding to TEAD such as VGLL4[49–51] and receptor tyrosine kinases such as the EGFR which can activate YAP/TAZ signaling by promoting LATS inactivation. In agreement, the EGFR inhibitor Erlotinib increased phospho-YAP and suppressed YAP/TAZ-regulated gene expression.[52] EGFR mediated activation of YAP may depend on EGF-like growth factors such as AREG which is also a target transcript regulated by YAP. YAP/TAZ can also interact with various non-TEAD transcription factors, including Smad2/3, Runx2, p63 and p73, and SOX2 to regulate gene expression.[24] Moreover, YAP binds to another transcriptional co-activator of the Wnt signaling pathway, β-catenin. Nuclear YAP upregulated the expression of β-catenin, while cytoplasmic YAP reduced its expression. In the absence of Wnt, free cytoplasmic β-catenin is degraded. Once Wnt signaling becomes activated, stabilized β-catenin accumulates and enters the nucleus where it acts as transcriptional co-activator for LEF/TCF transcription factors. Wnt signaling has been implicated in the regulation of epidermal stratification. In primary human keratinocytes, Wnt5a acts as an autocrine stimulus to promote extracellular calcium-induced keratinocyte differentiation.[53] Additionally, mechanical stress inhibits LATS1/2 kinase activity via Rho GTPase and the actin cytoskeleton.[54,55] PKP4-KO cells completely lost intrinsic tension and a cortical actin ring[19] due to reduced RhoA activity which is compatible with increased LATS phosphorylation and activation. Therefore, PKP4 may contribute to Hippo pathway control through mechanosignaling.

Finally, we find that YAP also regulated PKP4 by stabilizing the PKP4 protein. This feedback mechanism might fine-tune the role of PKP4 in balancing intercellular adhesion, proliferation, and differentiation via the Hippo and presumably the Polycomb repressive complex in response to diverse stimuli including cell density.

Limitations of the study

The continuous balance of proliferation and differentiation is essential for skin homeostasis. Our data indicate that PKP4 plays a crucial role in this context by dynamically regulating the Hippo signaling pathway primarily through its downstream modulator YAP. PKP4 had two opposing effects: On one hand, it inhibited Hippo signaling thereby promoting YAP nuclear localization and proliferation in undifferentiated cells, and on the other hand, upon commitment to differentiation, PKP4 recruited YAP to the junctional zone where YAP is transcriptionally inactive. We therefore propose that PKP4 plays a crucial role in balancing YAP-dependent proliferation with YAP-dependent junctional stabilization to regulate proliferation in basal cells and in transit-amplifying cells. So far, it is not entirely clear how these two aspects are balanced in the epidermis since our study did not specifically address the role of PKP4 in the intact epidermis. Adult PKP4-KO mice showed no obvious skin phenotype such as severe blistering or hair loss. However, further studies are required to characterize the epidermal morphology of PKP4-KO mice and to identify putative milder changes. Moreover, wound healing studies can reveal if PKP4 affects the complex healing process, which includes inflammation, proliferation, re-epithelialization, and re-modeling. The Hippo pathway interacts with numerous other pathways resulting in a high complexity in controlling cell behavior. Cell density, growth factor signaling, and mechanical clues all contribute to regulating this delicate equilibrium. Therefore, it will be interesting to assess how PKP4 affects the crosstalk between Hippo signaling and other pathways that coordinate proliferation and differentiation in an adhesion- and/or tension-dependent manner, including Polycomb complex, EGF receptor signaling, Wnt signaling, and cytoskeleton signaling via Rho GTPases. Finally, the Hippo pathway constitutes one of the top signaling pathways altered in human cancer.[56] Therefore, it will be interesting to unravel the involvement of PKP4 in modulating Hippo signaling and AJs in cancer. Linking the postulated tumor suppressor PKP4 to the Hippo signaling pathway adds an important new aspect of AJs function in regulating cell growth and differentiation.

RESOURCE AVAILABILITY

Lead contact

Further information and requests for resources and reagents should be directed to and will be fulfilled by the lead contact and corresponding author, L.M. (lisa.mueller@uk-halle.de).

Materials availability

This study did not generate new unique reagents.

Data and code availability

- All data reported in this paper will be shared by the lead contact upon request.
- This paper does not report original code.
- Any additional information required to reanalyze the data reported in this paper is available from the lead contact upon request.

ACKNOWLEDGMENTS

We thank Andrej Mun, Annekathrin Hedler, and Mario Riedel for technical assistance and Dr. Nadine Bley from the Core Facility Imaging (CFI) at the Martin Luther University for competent support with Incucyte proliferation analyses. This work was supported by the German Research Council (DFG) project Ha 1791/12-1 to M.H.. We acknowledge the financial support of the Open Access Publication Fund of the Martin Luther University Halle-Wittenberg.

AUTHOR CONTRIBUTIONS

L.M.: Conceptualization, Validation, Formal analysis, Investigation, Writing – Original Draft, Writing – Review and Editing, Visualization. **T.G.:** Writing – Review and Editing. **M.H.:** Conceptualization, Writing – Original Draft, Writing – Review and Editing, Supervision, Project administration, Funding acquisition.

DECLARATION OF INTERESTS

The authors declare no competing interests.

STAR★METHODS

Detailed methods are provided in the online version of this paper and include the following:

- KEY RESOURCES TABLE
- EXPERIMENTAL MODEL AND STUDY PARTICIPANT DETAILS
  - Isolation of *Pkp4*$^{+/+}$ and *Pkp4*$^{-/-}$ keratinocytes
  - Cell lines, cell culture, and treatments
  - Transfections
  - Plasmids and cloning
- METHOD DETAILS
  - BrdU assay
  - Cell cycle analyses
  - Cell proliferation assay
  - Cell size
  - Epithelial sheet assay (dispase assay)
  - Immunofluorescence analysis and image processing
  - Immunoprecipitation
  - Nucleus/cytoplasm fractionation
  - Protein extraction
  - RNA expression
  - SDS-PAGE and western blotting
  - Gene set enrichment analysis
- QUANTIFICATION AND STATISTICAL ANALYSIS
  - Western blot quantification
  - Quantification of immunofluorescence
  - Statistical analysis

SUPPLEMENTAL INFORMATION

Supplemental information can be found online at https://doi.org/10.1016/j.isci.2024.110762.

Received: March 27, 2024
Revised: July 12, 2024
Accepted: August 14, 2024
Published: August 19, 2024

REFERENCES

1. Boopathy, G.T.K., and Hong, W. (2019). Role of Hippo Pathway-YAP/TAZ Signaling in Angiogenesis. Front. Cell Dev. Biol. *7*, 49. https://doi.org/10.3389/fcell.2019.00049.
2. Ma, S., Meng, Z., Chen, R., and Guan, K.L. (2019). The Hippo Pathway: Biology and Pathophysiology. Annu. Rev. Biochem. *88*, 577–604. https://doi.org/10.1146/annurev-biochem-013118-111829.
3. Rognoni, E., and Walko, G. (2019). The Roles of YAP/TAZ and the Hippo Pathway in Healthy and Diseased Skin. Cells *8*, 411. https://doi.org/10.3390/cells8050411.
4. Zhang, H., Pasolli, H.A., and Fuchs, E. (2011). Yes-associated protein (YAP) transcriptional coactivator functions in balancing growth and differentiation in skin. Proc. Natl. Acad. Sci. USA *108*, 2270–2275. https://doi.org/10.1073/pnas.1019603108.
5. Yu, F.X., Zhao, B., and Guan, K.L. (2015). Hippo Pathway in Organ Size Control, Tissue Homeostasis, and Cancer. Cell *163*, 811–828. https://doi.org/10.1016/j.cell.2015.10.044.
6. Benham-Pyle, B.W., Pruitt, B.L., and Nelson, W.J. (2015). Cell adhesion. Mechanical strain

induces E-cadherin-dependent Yap1 and beta-catenin activation to drive cell cycle entry. Science *348*, 1024–1027. https://doi.org/10.1126/science.aaa4559.

7. Kim, N.G., Koh, E., Chen, X., and Gumbiner, B.M. (2011). E-cadherin mediates contact inhibition of proliferation through Hippo signaling-pathway components. Proc. Natl. Acad. Sci. USA *108*, 11930–11935. https://doi.org/10.1073/pnas.1103345108.
8. Schlegelmilch, K., Mohseni, M., Kirak, O., Pruszak, J., Rodriguez, J.R., Zhou, D., Kreger, B.T., Vasioukhin, V., Avruch, J., Brummelkamp, T.R., and Camargo, F.D. (2011). Yap1 acts downstream of alpha-catenin to control epidermal proliferation. Cell *144*, 782–795. https://doi.org/10.1016/j.cell.2011.02.031.
9. Silvis, M.R., Kreger, B.T., Lien, W.H., Klezovitch, O., Rudakova, G.M., Camargo, F.D., Lantz, D.M., Seykora, J.T., and Vasioukhin, V. (2011). alpha-catenin is a tumor suppressor that controls cell accumulation by regulating the localization and activity of the transcriptional coactivator Yap1. Sci. Signal. *4*, ra33. https://doi.org/10.1126/scisignal.2001823.
10. Keil, R., Schulz, J., and Hatzfeld, M. (2013). p0071/PKP4, a multifunctional protein coordinating cell adhesion with cytoskeletal organization. Biol. Chem. *394*, 1005–1017. https://doi.org/10.1515/hsz-2013-0114.
11. Setzer, S.V., Calkins, C.C., Garner, J., Summers, S., Green, K.J., and Kowalczyk, A.P. (2004). Comparative analysis of armadillo family proteins in the regulation of a431 epithelial cell junction assembly, adhesion and migration. J. Invest. Dermatol. *123*, 426–433. https://doi.org/10.1111/j.0022-202X.2004.23319.x.
12. Hofmann, I., Kuhn, C., and Franke, W.W. (2008). Protein p0071, a major plaque protein of non-desmosomal adhering junctions, is a selective cell-type marker. Cell Tissue Res. *334*, 381–399. https://doi.org/10.1007/s00441-008-0725-2.
13. Perez-Moreno, M., Davis, M.A., Wong, E., Pasolli, H.A., Reynolds, A.B., and Fuchs, E. (2006). p120-catenin mediates inflammatory responses in the skin. Cell *124*, 631–644. https://doi.org/10.1016/j.cell.2005.11.043.
14. Calkins, C.C., Hoepner, B.L., Law, C.M., Novak, M.R., Setzer, S.V., Hatzfeld, M., and Kowalczyk, A.P. (2003). The Armadillo family protein p0071 is a VE-cadherin- and desmoplakin-binding protein. J. Biol. Chem. *278*, 1774–1783. https://doi.org/10.1074/jbc.M205693200.
15. Holstein, T.W., and David, C.N. (1990). Cell cycle length, cell size, and proliferation rate in hydra stem cells. Dev. Biol. *142*, 392–400. https://doi.org/10.1016/0012-1606(90)90360-u.
16. Brown, G., Hughes, P.J., and Michell, R.H. (2003). Cell differentiation and proliferation–simultaneous but independent? Exp. Cell Res. *291*, 282–288. https://doi.org/10.1016/s0014-4827(03)00393-8.
17. Cho, I.J., Lui, P.P., Obajdin, J., Riccio, F., Stroukov, W., Willis, T.L., Spagnoli, F., and Watt, F.M. (2019). Mechanisms, Hallmarks, and Implications of Stem Cell Quiescence. Stem Cell Rep. *12*, 1190–1200. https://doi.org/10.1016/j.stemcr.2019.05.012.
18. Fuchs, E. (1993). Epidermal differentiation and keratin gene expression. J. Cell Sci. Suppl. *17*, 197–208. https://doi.org/10.1242/jcs.1993.supplement_17.28.
19. Müller, L., Keil, R., Glaß, M., and Hatzfeld, M. (2024). Plakophilin 4 controls the spatio-temporal activity of RhoA at adherens junctions to promote cortical actin ring formation and tissue tension. Cell. Mol. Life Sci. *81*, 291. https://doi.org/10.1007/s00018-024-05329-6.
20. The Gene Ontology Consortium (2019). The Gene Ontology Resource: 20 years and still GOing strong. Nucleic Acids Res. *47*, D330–D338. https://doi.org/10.1093/nar/gky1055.
21. Mo, J.S., Park, H.W., and Guan, K.L. (2014). The Hippo signaling pathway in stem cell biology and cancer. EMBO Rep. *15*, 642–656. https://doi.org/10.15252/embr.201438638.
22. Reggiani, F., Gobbi, G., Ciarrocchi, A., and Sancisi, V. (2021). YAP and TAZ Are Not Identical Twins. Trends Biochem. Sci. *46*, 154–168. https://doi.org/10.1016/j.tibs.2020.08.012.
23. Kofler, M., and Kapus, A. (2023). Nuclear Import and Export of YAP and TAZ. Cancers *15*, 4956. https://doi.org/10.3390/cancers15204956.
24. Heng, B.C., Zhang, X., Aubel, D., Bai, Y., Li, X., Wei, Y., Fussenegger, M., and Deng, X. (2020). Role of YAP/TAZ in Cell Lineage Fate Determination and Related Signaling Pathways. Front. Cell Dev. Biol. *8*, 735. https://doi.org/10.3389/fcell.2020.00735.
25. Ahmad, U.S., Uttagomol, J., and Wan, H. (2022). The Regulation of the Hippo Pathway by Intercellular Junction Proteins. Life *12*, 1792. https://doi.org/10.3390/life12111792.
26. Mendonsa, A.M., Na, T.Y., and Gumbiner, B.M. (2018). E-cadherin in contact inhibition and cancer. Oncogene *37*, 4769–4780. https://doi.org/10.1038/s41388-018-0304-2.
27. Bunker, E.N., Wheeler, G.E., Chapnick, D.A., and Liu, X. (2021). Suppression of alpha-catenin and adherens junctions enhances epithelial cell proliferation and motility via TACE-mediated TGF-alpha autocrine/paracrine signaling. Mol. Biol. Cell *32*, 348–361. https://doi.org/10.1091/mbc.E19-08-0474.
28. Lin, W.H., Cooper, L.M., and Anastasiadis, P.Z. (2023). Cadherins and catenins in cancer: connecting cancer pathways and tumor microenvironment. Front. Cell Dev. Biol. *11*, 1137013. https://doi.org/10.3389/fcell.2023.1137013.
29. Perez-Moreno, M., Song, W., Pasolli, H.A., Williams, S.E., and Fuchs, E. (2008). Loss of p120 catenin and links to mitotic alterations, inflammation, and skin cancer. Proc. Natl. Acad. Sci. USA *105*, 15399–15404. https://doi.org/10.1073/pnas.0807301105.
30. Ke, C., Bandyopadhyay, D., and Sarkar, D. (2023). Gene Screening for Prognosis of Non-Muscle-Invasive Bladder Carcinoma under Competing Risks Endpoints. Cancers *15*, 379. https://doi.org/10.3390/cancers15020379.
31. Eisenhoffer, G.T., Loftus, P.D., Yoshigi, M., Otsuna, H., Chien, C.B., Morcos, P.A., and Rosenblatt, J. (2012). Crowding induces live cell extrusion to maintain homeostatic cell numbers in epithelia. Nature *484*, 546–549. https://doi.org/10.1038/nature10999.
32. Marinari, E., Mehonic, A., Curran, S., Gale, J., Duke, T., and Baum, B. (2012). Live-cell delamination counterbalances epithelial growth to limit tissue overcrowding. Nature *484*, 542–545. https://doi.org/10.1038/nature10984.
33. Mesa, K.R., Kawaguchi, K., Cockburn, K., Gonzalez, D., Boucher, J., Xin, T., Klein, A.M., and Greco, V. (2018). Homeostatic Epidermal Stem Cell Self-Renewal Is Driven by Local Differentiation. Cell Stem Cell *23*, 677–686.e4. https://doi.org/10.1016/j.stem.2018.09.005.
34. Cancedda, R., and Mastrogiacomo, M. (2023). Transit Amplifying Cells (TACs): a still not fully understood cell population. Front. Bioeng. Biotechnol. *11*, 1189225. https://doi.org/10.3389/fbioe.2023.1189225.
35. Hsu, Y.C., Li, L., and Fuchs, E. (2014). Transit-amplifying cells orchestrate stem cell activity and tissue regeneration. Cell *157*, 935–949. https://doi.org/10.1016/j.cell.2014.02.057.
36. Beverdam, A., Claxton, C., Zhang, X., James, G., Harvey, K.F., and Key, B. (2013). Yap controls stem/progenitor cell proliferation in the mouse postnatal epidermis. J. Invest. Dermatol. *133*, 1497–1505. https://doi.org/10.1038/jid.2012.430.
37. Debaugnies, M., Sánchez-Danes, A., Rorive, S., Raphael, M., Liagre, M., Parent, M.A., Brisebarre, A., Salmon, I., and Blanpain, C. (2018). YAP and TAZ are essential for basal and squamous cell carcinoma initiation. EMBO Rep. *19*, e45809. https://doi.org/10.15252/embr.201845809.
38. Oh, H., Slattery, M., Ma, L., Crofts, A., White, K.P., Mann, R.S., and Irvine, K.D. (2013). Genome-wide association of Yorkie with chromatin and chromatin-remodeling complexes. Cell Rep. *3*, 309–318. https://doi.org/10.1016/j.celrep.2013.01.008.
39. Oh, H., Slattery, M., Ma, L., White, K.P., Mann, R.S., and Irvine, K.D. (2014). Yorkie promotes transcription by recruiting a histone methyltransferase complex. Cell Rep. *8*, 449–459. https://doi.org/10.1016/j.celrep.2014.06.017.
40. Stein, C., Bardet, A.F., Roma, G., Bergling, S., Clay, I., Ruchti, A., Agarinis, C., Schmelzle, T., Bouwmeester, T., Schübeler, D., and Bauer, A. (2015). YAP1 Exerts Its Transcriptional Control via TEAD-Mediated Activation of Enhancers. PLoS Genet. *11*, e1005465. https://doi.org/10.1371/journal.pgen.1005465.
41. Cohen, I., Bar, C., Liu, H., Valdes, V.J., Zhao, D., Galbo, P.M., Jr., Silva, J.M., Koseki, H., Zheng, D., and Ezhkova, E. (2021). Polycomb complexes redundantly maintain epidermal stem cell identity during development. Genes Dev. *35*, 354–366. https://doi.org/10.1101/gad.345363.120.
42. Blackledge, N.P., and Klose, R.J. (2021). The molecular principles of gene regulation by Polycomb repressive complexes. Nat. Rev. Mol. Cell Biol. *22*, 815–833. https://doi.org/10.1038/s41580-021-00398-y.
43. Ezhkova, E., Lien, W.H., Stokes, N., Pasolli, H.A., Silva, J.M., and Fuchs, E. (2011). EZH1 and EZH2 cogovern histone H3K27 trimethylation and are essential for hair follicle homeostasis and wound repair. Genes Dev. *25*, 485–498. https://doi.org/10.1101/gad.2019811.
44. Ezhkova, E., Pasolli, H.A., Parker, J.S., Stokes, N., Su, I.H., Hannon, G., Tarakhovsky, A., and Fuchs, E. (2009). Ezh2 orchestrates gene expression for the stepwise differentiation of tissue-specific stem cells. Cell *136*, 1122–1135. https://doi.org/10.1016/j.cell.2008.12.043.
45. Torigata, K., Daisuke, O., Mukai, S., Hatanaka, A., Ohka, F., Motooka, D., Nakamura, S., Ohkawa, Y., Yabuta, N., Kondo, Y., and Nojima, H. (2016). LATS2 Positively Regulates Polycomb Repressive Complex 2. PLoS One *11*, e0158562. https://doi.org/10.1371/journal.pone.0158562.

46. Hoxha, S., Shepard, A., Troutman, S., Diao, H., Doherty, J.R., Janiszewska, M., Witwicki, R.M., Pipkin, M.E., Ja, W.W., Kareta, M.S., and Kissil, J.L. (2020). YAP-Mediated Recruitment of YY1 and EZH2 Represses Transcription of Key Cell-Cycle Regulators. Cancer Res. *80*, 2512–2522. https://doi.org/10.1158/0008-5472.CAN-19-2415.
47. Vieux-Rochas, M., Fabre, P.J., Leleu, M., Duboule, D., and Noordermeer, D. (2015). Clustering of mammalian Hox genes with other H3K27me3 targets within an active nuclear domain. Proc. Natl. Acad. Sci. USA *112*, 4672–4677. https://doi.org/10.1073/pnas.1504783112.
48. Liu, M., Zhao, S., Lin, Q., and Wang, X.P. (2015). YAP regulates the expression of Hoxa1 and Hoxc13 in mouse and human oral and skin epithelial tissues. Mol. Cell Biol. *35*, 1449–1461. https://doi.org/10.1128/MCB.00765-14.
49. Zhang, W., Gao, Y., Li, P., Shi, Z., Guo, T., Li, F., Han, X., Feng, Y., Zheng, C., Wang, Z., et al. (2014). VGLL4 functions as a new tumor suppressor in lung cancer by negatively regulating the YAP-TEAD transcriptional complex. Cell Res. *24*, 331–343. https://doi.org/10.1038/cr.2014.10.
50. Lin, Z., Guo, H., Cao, Y., Zohrabian, S., Zhou, P., Ma, Q., VanDusen, N., Guo, Y., Zhang, J., Stevens, S.M., et al. (2016). Acetylation of VGLL4 Regulates Hippo-YAP Signaling and Postnatal Cardiac Growth. Dev. Cell *39*, 466–479. https://doi.org/10.1016/j.devcel.2016.09.005.
51. Deng, X., and Fang, L. (2018). VGLL4 is a transcriptional cofactor acting as a novel tumor suppressor via interacting with TEADs. Am. J. Cancer Res. *8*, 932–943.
52. Ando, T., Arang, N., Wang, Z., Costea, D.E., Feng, X., Goto, Y., Izumi, H., Gilardi, M., Ando, K., and Gutkind, J.S. (2021). EGFR Regulates the Hippo pathway by promoting the tyrosine phosphorylation of MOB1. Commun. Biol. *4*, 1237. https://doi.org/10.1038/s42003-021-02744-4.
53. Veltri, A., Lang, C., and Lien, W.H. (2018). Concise Review: Wnt Signaling Pathways in Skin Development and Epidermal Stem Cells. Stem Cell. *36*, 22–35. https://doi.org/10.1002/stem.2723.
54. Wada, K.I., Itoga, K., Okano, T., Yonemura, S., and Sasaki, H. (2011). Hippo pathway regulation by cell morphology and stress fibers. Development *138*, 3907–3914. https://doi.org/10.1242/dev.070987.
55. Zhao, B., Li, L., Wang, L., Wang, C.Y., Yu, J., and Guan, K.L. (2012). Cell detachment activates the Hippo pathway via cytoskeleton reorganization to induce anoikis. Genes Dev. *26*, 54–68. https://doi.org/10.1101/gad.173435.111.
56. Sanchez-Vega, F., Mina, M., Armenia, J., Chatila, W.K., Luna, A., La, K.C., Dimitriadoy, S., Liu, D.L., Kantheti, H.S., Saghafinia, S., et al. (2018). Oncogenic Signaling Pathways in The Cancer Genome Atlas. Cell *173*, 321–337.e10. https://doi.org/10.1016/j.cell.2018.03.035.
57. Schindelin, J., Arganda-Carreras, I., Frise, E., Kaynig, V., Longair, M., Pietzsch, T., Preibisch, S., Rueden, C., Saalfeld, S., Schmid, B., et al. (2012). Fiji: an open-source platform for biological-image analysis. Nat. Methods *9*, 676–682. https://doi.org/10.1038/nmeth.2019.
58. Rietscher, K., Wolf, A., Hause, G., Rother, A., Keil, R., Magin, T.M., Glass, M., Niessen, C.M., and Hatzfeld, M. (2016). Growth Retardation, Loss of Desmosomal Adhesion, and Impaired Tight Junction Function Identify a Unique Role of Plakophilin 1 In Vivo. J. Invest. Dermatol. *136*, 1471–1478. https://doi.org/10.1016/j.jid.2016.03.021.
59. Müller, L., Keil, R., and Hatzfeld, M. (2023). Plakophilin 3 facilitates G1/S phase transition and enhances proliferation by capturing RB protein in the cytoplasm and promoting EGFR signaling. Cell Rep. *42*, 112031. https://doi.org/10.1016/j.celrep.2023.112031.
60. Müller, L., Rietscher, K., Keil, R., Neuholz, M., and Hatzfeld, M. (2020). Plakophilin 3 phosphorylation by ribosomal S6 kinases supports desmosome assembly. J. Cell Sci. *133*, jcs238295. https://doi.org/10.1242/jcs.238295.

STAR★METHODS

KEY RESOURCES TABLE

REAGENT or RESOURCE	SOURCE	IDENTIFIER
Antibodies		
Filaggrin rabbit polyclonal antibody	Santa Cruz Biotechnology	Cat# sc-30230
GAPDH mouse monoclonal antibody	Sigma-Aldrich	Cat# 8795
GFP rabbit polyclonal antibody	Rockland	Cat# 600-401-215; RRID: AB_828167
Involucrin mouse monoclonal antibody	Santa Cruz Biotechnology	Cat# sc-21748
Keratin 1 rabbit polyclonal customized peptide specific antibody	Peptide Specialty Laboratories	N/A
Keratin 10 rabbit polyclonal customized peptide specific antibody	Peptide Specialty Laboratories	N/A
Keratin 14 rabbit polyclonal customized peptide specific antibody	Peptide Specialty Laboratories	N/A
Keratin 17 rabbit polyclonal customized peptide specific antibody	Peptide Specialty Laboratories	N/A
LATS1 rabbit monoclonal antibody	Cell Signaling Technology	Cat# 3477
Loricrin rabbit polyclonal antibody	GeneTex	Cat# GTX116013; RRID: AB_2037360
P54 (nrb) mouse monoclonal antibody	BD Transduction Laboratories	Cat# 611279; RRID: AB_398807
P-H3-Ser10 rabbit monoclonal antibody	Cell Signaling Technology	Cat# 3377
P-LATS-Thr1079 rabbit monoclonal antibody	Cell Signaling Technology	Cat# 8654
P-MST1-Thr183/P-MST2-Thr180 rabbit monoclonal antibody	Cell Signaling Technology	Cat# 49332
P-RB-Ser807/811 rabbit monoclonal antibody	Cell Signaling Technology	Cat# 8516
P-YAP-Ser127 rabbit monoclonal antibody	Cell Signaling Technology	Cat# 13008
PKP4 mouse monoclonal antibody	Progen	Cat# 651166
SAV1 rabbit monoclonal antibody	Cell Signaling Technology	Cat# 13301
TAZ rabbit monoclonal antibody	Cell Signaling Technology	Cat# 83669
YAP rabbit monoclonal antibody	Cell Signaling Technology	Cat# 14074
YAP/TAZ rabbit monoclonal antibody	Cell Signaling Technology	Cat# 8418
α-tubulin mouse monoclonal antibody	Sigma-Aldrich	Cat# T9026
Alexa Fluor® 488 AffiniPure F(ab')$_2$ Fragment Donkey Anti-Mouse IgG	Jackson ImmunoResearch	Cat# 715-546-150; RRID: AB_2340849
Cy™3 AffiniPure F(ab')$_2$ Fragment Donkey Anti-Rabbit IgG	Jackson ImmunoResearch	Cat# 711-166-152, RRID: AB_2313568
Normal rabbit IgG	Santa Cruz Biotechnology	Cat# sc-2027 (discontinued)
Peroxidase AffiniPure Donkey Anti-Mouse IgG	Jackson ImmunoResearch	Cat# 715-035-150; RRID: AB_2340770
Peroxidase AffiniPure Donkey Anti-Rabbit IgG	Jackson ImmunoResearch	Cat# 711-035-152; RRID: AB_10015282
Bacterial and virus strains		
E. coli JM109	Promega	Cat# P9751
Chemicals, peptides, and recombinant proteins		
Adenine	Sigma-Aldrich	Cat# A8626-5G
Ala-Gln solution, 200 mM	Sigma-Aldrich	Cat# G8541
Benzonase	Santa Cruz Biotechnology	Cat# sc-202391
Chelex 100 Chelating Resin	Bio-Rad	Cat# 142-2842
Choleratoxin	Sigma-Aldrich	Cat# C8052

(*Continued on next page*)

Continued

REAGENT or RESOURCE	SOURCE	IDENTIFIER
Collagen I, Rat Tail	Corning	Cat# 354236
Cycloheximide	Sigma-Adrich	Cat# 239763
D-(+)-Glucose solution, 45%	Sigma-Aldrich	Cat# G8769
1,4- diazabicyclo[2.2.2]octane (DABCO)	Sigma-Aldrich	Cat# D27802
Dispase II	Roche Diagnostics	Cat# 04942078001
DMEM, 4.5 g/l high glucose	Sigma-Aldrich	Cat# D6429
DMEM/Ham's F12 (3.5:1.1) medium containing 50 µM $CaCl_2$; customized formulation, w/o: Glucose, w/o: L-Glutamine, w/o:Phenol red, w/o: Sodium pyruvate, w: 3.096 g/L $NaHCO_3$	Pan-Biotech	N/A
Epidermal growth factor	Sigma-Aldrich	Cat# E4127
Ethylene glycol-bis(β-aminoethyl ether)-*N*,*N*,*N*′,*N*′-tetraacetic acid (EGTA)	Sigma-Aldrich	Cat# E3889
Fetal Bovine Serum (FBS) Superior	Sigma-Aldrich	Cat# S0615
GFP-Trap Agarose	Chromotek	Cat# gta-20
Halt™ protease and phosphatase inhibitor cocktail	Thermo Fisher Scientific	Cat# 78444
Hoechst 33342	Thermo Fisher Scientific	Cat# H1399
Hydrocortisone	Sigma-Aldrich	Cat# H4001-1G
4-(2-hydroxyethyl)-1-piperazineethanesulfonic acid (HEPES)	Sigma-Aldrich	Cat# H0887
Insulin solution	Sigma-Aldrich	Cat# I9278
Lenti-X concentrator	Takara Bio	Cat# 631232
Lipofectamine® RNAiMax	Thermo Fisher Scientific	Cat# 13778150
Mowiol® 4-88	Sigma-Aldrich	Cat# 81381
Pierce™ Protein A Plus Agarose	Thermo Fisher Scientific	Cat# 22811
Propidium iodide	Thermo Fisher Scientific	Cat# P3566
Puromycin dihydrochloride from *Streptomyces alboniger*	Sigma-Aldrich	Cat# P8833
2x QPCR CYBRGreen Master Mix	Steinbrenner-Laborsysteme GmbH	Cat# SL-9902
Random hexamer primers	Thermo Fisher Scientific	Cat# SO142
RNase A	Sigma-Aldrich	Cat# 10109142001
Sodium pyruvate solution, 100 mM	Sigma-Aldrich	Cat# S8636
SuperScript® II Reverse Transcriptase	Thermo Fisher Scientific	Cat# 18064014
Trypsin (2,5 %)	Thermo Fisher Scientific	Cat# 15090046
Western Blot Ultra-Sensitive HRP Substrate	Takara Bio	Cat# T7104A
Critical commercial assays		
Cell Proliferation ELISA, BrdU (colorimetric)	Sigma-Aldrich	Cat# 11647229001
Pierce™ BCA Protein Assay Kit	Thermo Fisher Scientific	Cat# 23225
Deposited data		
RNA-sequencing	Müller et al.[19]	NCBI GEO accession: GSE255172
Experimental models: Cell lines		
Hek293T	Kindly provided by Stefan Hüttelmaier	N/A
WT keratinocytes (murine keratinocytes *PKP4*$^{+/+}$)	This paper	N/A
PKP4-KO keratinocytes (murine keratinocytes *PKP4*$^{-/-}$)	This paper	N/A
PKP4-KO+PKP4 keratinocytes (murine keratinocytes *PKP4*$^{-/-}$ expressing EGFP-PKP4-WT)	This paper	N/A

(*Continued on next page*)

Continued

REAGENT or RESOURCE	SOURCE	IDENTIFIER
WT+GFP keratinocytes (murine keratinocytes *PKP4*$^{+/+}$ expressing EGFP)	This paper	N/A
Experimental models: Organisms/strains		
Mouse: B6;SJL-Tg(ACTFLPe)9205Dym/J	The Jackson Laboratory	RRID: IMSR_JAX:003800
Mouse: C57BL/6J	The Jackson Laboratory	RRID: IMSR_JAX:000664
Mouse: C57BL/6N-Pkp4$^{tm1b(EUCOMM)Wtsi}$/JMmucd	Mutant Mouse Resource and Research Center	RRID: MMRRC_049090-UCD
Oligonucleotides		
qRT-PCR-Primer (Table S4)	This paper	N/A
siPools (Table S1)	siTools Biotech	N/A
Recombinant DNA		
EGFP-pLVX-IRES-puro	This paper	N/A
EGFP-PKP4-WT-pLVX-IRES-puro	This paper	N/A
pMD2.G	Kindly provided by Didier Trono	Addgene plasmid #12259
psPAX2	Kindly provided by Didier Trono	Addgene plasmid #12260
Software and algorithms		
BioRender	BioRender	https://biorender.com/
IncuCyte® S3 Software (version 2021C, Sartorius)	Satorius	https://www.sartorius.com/en/products/live-cell-imaging-analysis/live-cell-analysis-instruments/s3-live-cell-analysis-instrument
Fiji (ImageJ)	Schindelin et al.[57]	https://imagej.net/software/fiji/downloads
FlowJo™ Software (version 10.6.0)	BD Biosciences	https://www.flowjo.com/solutions/flowjo/downloads
MACSQuantify™ Software (version 2.11)	Miltenyi Biotec	Cat# 130-094-556
NIS-Elements AR software (version 4.12.00)	Nikon	https://www.microscope.healthcare.nikon.com/en_EU/products/software/nis-elements
Prism 8.3	GraphPad Software	https://www.graphpad.com/scientific-software/prism/
TC20 data analyzer	BioRad	https://www.bio-rad.com/webroot/web/html/lsr/products/cell_counting/product_overlay/global/tc20-data-ana.html

EXPERIMENTAL MODEL AND STUDY PARTICIPANT DETAILS

Isolation of *Pkp4*$^{+/+}$ and *Pkp4*$^{-/-}$ keratinocytes

The mouse strain used for this research project, C57BL/6N-Pkp4$^{tm1b(EUCOMM)Wtsi}$/JMmucd, RRID: MMRRC_049090-UCD, was obtained from the Mutant Mouse Resource and Research Center (MMRRC) at University of California at Davis, an NIH-funded strain repository, and was donated to the MMRRC by The KOMP Repository, University of California, Davis; Originating from Stephen Murray, The Jackson Laboratory. C57BL/6N-Pkp4$^{tm1b(EUCOMM)Wtsi}$/JMmucd was generated by Cre-mediated excision of the parental Pkp4$^{tm1a(EUCOMM)Wtsi}$ allele resulted in the removal of the promoter-driven neomycin selection cassette and critical exon 9, leaving behind the inserted lacZ reporter sequence. The reporter sequence was removed by breeding with B6;SJL-Tg(ACTFLPe)9205Dym/J (RRID: IMSR_JAX:003800) mice and resulting post-Cre / post-FLPe mice were backcrossed onto the C57BL/6J (RRID: IMSR_JAX:000664) background for 10 backcross generations. Thereafter Pkp4$^{+/-}$ siblings were intercrossed to generate Pkp4$^{+/+}$ and Pkp4$^{-/-}$ animals. All animal experiments were approved by the local authorities (Landesverwaltungsamt Sachsen-Anhalt, reference number 42502-2-1482 MLU).

Primary keratinocytes of Pkp4$^{+/+}$ mice (female) and Pkp4$^{-/-}$ mice (male) were isolated from newborn (age 1 day) pups, essentially as described.[58] Briefly, the dissected skin was incubated with 5 mg/ml Dispase (Roche diagnostics, Mannheim, Germany) in PBS overnight at 4°C to separate the epidermis from the dermis. Subsequently, the epidermal sheet was incubated in trypsin solution (0.025% trypsin in PBS/ 0.02% EDTA) for 10min at 37°C to liberate the keratinocytes (hereafter PKP4-WT and PKP4-KO).

Cell lines, cell culture, and treatments

HEK293T cells were grown in Dulbeccoś modified Eagleś medium [DMEM, 4.5 g/l high glucose, 1 mM sodium pyruvate, 1 mM glutamate, 10% (v/v) fetal calf serum (FCS)] at 37°C in 5% CO_2 and 90% humidity. Mouse keratinocytes were grown on 15 μg/ml collagen I (Corning, Glendale, Arizona, USA) in LCM [DMEM/Ham's F12 medium containing 50 μM $CaCl_2$, 10% (v/v) Ca^{2+} free FCS, 1 mM sodium pyruvate, 1 mM glutamate, 0.18 mM adenine, 0.5 μg/ml hydrocortisone, 5 μg/ml insulin, 10 ng/ml EGF, 100 pM cholera toxin, 1 mg/ml D-(+)-glucose] at 32°C in 5% CO_2 and 90% humidity.

To generate PKP4-KO keratinocytes expressing EGFP-PKP4-WT (PKP4-KO+PKP4 rescue cells) and WT cells expressing EGFP (GFP cells), HEK293T cells were co-transfected by $CaPO_4$ precipitation with the packaging plasmids pMD2.G (Addgene plasmid #12259; gift from Didier Trono), psPAX2 (Addgene plasmid #12260; gift from Didier Trono), and lentiviral expression vector pLVX-IRES-puro encoding either EGFP or human PKP4 N-terminally tagged with EGFP. Lentiviral particles were purified 48h after transfection using Lenti-X concentrator (Takara Bio Inc., Kusatsu, Shiga, Japan) according to the manufacturerś protocol. Keratinocytes were incubated with the lentiviral particles for 24h and subsequently selected using puromycin (1 μg/ml) to obtain stable cell lines. The resulting cell lines were analyzed by fluorescence microscopy and western blotting to monitor expression of transgenes.

To induce the differentiation of keratinocytes, LCM was supplemented with 1.2 mM $CaCl_2$ (HCM).

For analysis of protein stability, keratinocytes were treated with 200 μg/ml CHX (Sigma-Aldrich) for 2h, 4h, or 8h and harvested at the indicated times. Samples were separated by sodium dodecyl sulfate (SDS) polyacrylamide gel electrophoresis (PAGE) and analyzed by western blotting.

Transfections

siRNA pools (defined pools of 30 selected siRNAs, Table S1) were obtained from siTools Biotech GmbH (Martinsried, Germany) and transfected using Lipofectamine® RNAiMax (Thermo Fisher Scientific, Waltham, MA, USA) according to the manufacturer's instructions. Keratinocytes transfected in suspension with 2 pmol of the respective siRNA pools were maintained in LCM for 72h or switched to HCM at 48h after transfection and kept in HCM for another 24h.

Plasmids and cloning

Human cDNA of PKP4-WT was subcloned into pLVX-IRES-puro (Takara Bio Inc.) containing an EGFP ORF. Vectors for the production of lentiviral particles pMD2.G and psPAX2 were a gift from Didier Trono (Addgene plasmids #12259, #12260). All constructs were validated by sequencing.

METHOD DETAILS

BrdU assay

To analyze DNA replication, a colorimetric BrdU assay was performed using the Cell Proliferation ELISA, BrdU Kit (Sigma-Aldrich) according to the manufacturer's instructions. Briefly, cells maintained in LCM or HCM for 24h, 48h, and 72h were incubated with BrdU (100 μM) for 6h at 32°C. Cells were fixed for 30min at room temperature using the fixation solution provided in the kit, incubated with the anti-BrdU peroxidase-coupled antibody for 90min, and washed three times with PBS to remove unbound antibodies. Tetramethylbenzidine-containing substrate solution was added for 100min until color development was sufficient for photometric detection. The absorbance of all samples was measured at 370 nm (reference wavelength 492 nm) using a plate reader Infinite® M PLEX (Tecan, Maennedorf, Switzerland). The blank control (assay performed in wells without cells) was subtracted from all other values.

Cell cycle analyses

For cell cycle analyses, cells were seeded at low density (10,000/cm^2). Cells were harvested by trypsinization at the indicated time points, washed, and fixed overnight in 70% ethanol at -20°C. Cells were pelleted by centrifugation (5min at room temperature at 3,200 *g*), washed three times with phosphate buffered saline (PBS), and incubated with 40 μg/ml RNAse A (Sigma-Aldrich) containing propidium iodide DNA-staining solution [1 mg/ml sodium citrate, 0.1 mM EDTA, 50 μg/ml propidium iodide (Sigma-Aldrich)] at 37°C for 10min in the dark. The DNA content of approximately 10,000 cells per sample was measured by flow cytometry using a MACSQuant® flow cytometer and the MACSQuantify™ Software (version 2.11, Miltenyi Biotec, Bergisch-Gladbach, Germany). The results were analyzed using FlowJo™ Software (version 10.6.0, Ashland, OR: Becton, Dickinson and Company).

Cell proliferation assay

For the assessment of cell proliferation in 2D culture, cells were seeded at low density (10,000/cm^2) and were grown for up to 96h. Live cell images were automatically taken 4h after seeding and then every 8h by using an IncuCyte® S3 System (Sartorius, Goettingen, Germany) with 20x magnification and the corresponding IncuCyte® S3 Software (version 2021C, Sartorius). For analysis of proliferation, phase images were masked to distinguish between background and nuclei using the basic analyzer provided by the Incucte® S3 Software. Cell proliferation was determined by analyzing the occupied area of individual nuclei over time.

Cell size

For analysis of cell size, keratinocytes were grown for 24h in LCM and harvested by trypsinization. The cell diameter was automatically measured using the BioRad TC20 Cell Counter (Bio-Rad Laboratories, Feldkirchen, Germany) and analyzed using the corresponding software (TC20 data analyzer, BioRad).

Epithelial sheet assay (dispase assay)

For analysis of intercellular cohesion in combination with knockdown, WT and PKP4-KO keratinocytes transfected with non-targeting (Ctrl), YAP-, or TAZ-directed siRNA-pools, were switched to HCM at 48h after transfection and kept in HCM for another 24h before incubation with 2.4 U/ml dispase II (Roche Diagnostics, Indianapolis, IN, USA) in DMEM/Ham's F12 medium supplemented with 1.2 mM Ca^{2+} and 25 mM HEPES for 30min at 37°C. After detachment, monolayers were kept for additional 30min in DMEM/Ham's F12 medium containing 1.2 mM Ca^{2+}, 25 mM HEPES and 3.3 mM ethylene bis(oxyethylenenitrilo)tetraacetic acid (EGTA) before submitting to mechanical stress on an orbital shaker at 750 *rpm*. Images were taken using a Sony DSC-H300 camera. For image processing and counting of fragments the ImageJ tool "Cell counter" was used.

Immunofluorescence analysis and image processing

Cells were grown on 12-mm collagen I-coated glass coverslips and fixed for 10min in methanol at -20°C or for 20min in 3.7% (w/v) formaldehyde in PBS on ice or at room temperature, permeabilized in detergent buffer [100 mM PIPES (pH 6.9), 4 M glycerol, 2 mM EDTA, 1 mM EGTA, 0.5% (v/v) Triton X-100] for 15min at room temperature, and blocked in 1% (w/v) BSA/PBS for 30min at room temperature. Primary antibodies were diluted in blocking solution and incubated overnight at 4°C in a humid chamber. The next day, coverslips were washed in PBS, briefly blocked, and incubated for 1h at room temperature with the fluorophore-conjugated secondary antibody. DNA was stained with Hoechst 33342 (Thermo Fisher Scientific). Antibodies used for immunofluorescence are listed in Tables S2 and S3. Coverslips were mounted in Mowiol [5% (w/v) Mowiol, 30% (v/v) glycerol, 0.25% (w/v) 1,4- diazabicyclo[2.2.2]octane (DABCO)]. Images were taken using a Nikon Eclipse E600 microscope, a CCD camera, and a Plan APO 60xA/1.40 oil objective controlled by the NIS-Elements AR software (version 4.12.00). Confocal images of keratin 1 were acquired on a confocal microscope (Leica SP8X) equipped with a white light laser, HyD detectors using a 63x/1.40 oil objective and Leica LAS AF software (Leica Microsystems, Wetzlar, Germany). For comparisons between WT, PKP4-KO, and Rescue cells, samples were treated in parallel and images captured at the same exposure times. Fiji software was used for image processing.[57]

Immunoprecipitation

All steps of the immunoprecipitation reactions were performed on ice. Cells were lysed in immunoprecipitation-buffer [20 mM Tris-HCl pH 7.5, 137 mM NaCl, 2 mM EDTA, 10% (v/v) glycerol, 1% (v/v) NP-40; supplemented with 1x Halt™ protease and phosphatase inhibitor cocktail]. Lysates were cleared by centrifugation for 15min at 4°C and 13,000 *g*. One-sixth of the lysate was mixed with SDS-PAGE loading buffer and stored at -20°C as an input control. The residual lysate was incubated with anti-YAP or anti-TAZ (Cell Signaling Technology, respectively) antibody overnight at 4°C on an overhead rotator. Normal rabbit IgG (Santa Cruz) was used as an isotype control. Protein A agarose beads (Thermo Fisher Scientific) were washed in immunoprecipitation buffer and added to the lysate for 1h at 4°C on an overhead rotator. Lysates were centrifuged for 3min at 4°C and 4,000 *g*, washed three times in immunoprecipitation buffer, and bound proteins eluted in SDS-PAGE loading buffer.

For GFP-Trap experiments, cells expressing a GFP-tagged protein were treated as described above. The obtained cell lysates were incubated with GFP-Trap Agarose (ChromoTek, Planegg, Germany) for 1h at 4°C on an overhead rotator, washed as described above, and eluted in SDS-PAGE loading buffer. In either case, input and eluate samples were separated by SDS-PAGE and analyzed by western blotting.

Nucleus/cytoplasm fractionation

All preparation steps were performed on ice. Cells were lysed in hypotonic buffer A [10 mM HEPES (pH 7.9), 10 mM KCl, 0.1 mM EDTA, 0.1 mM EGTA; supplemented with 1x Halt™ protease and phosphatase inhibitor cocktail and 0.5 mM DTT] and incubated for 10min on an orbital shaker at 600 U/min. NP-40 was added to a final concentration of 3%. The resulting solutions were kept for 10min. Cells were homogenized using hypodermic needles (0.45 x 25 mm) and up and down passes of the syringe for 10 iterations. Lysates were cleared by centrifugation for 30 sec at 4°C and 14,000 *g*. The supernatant was collected as the cytoplasmic fraction and stored at -20°C. The pellet was washed three times in buffer A and incubated in hypertonic buffer C [20 mM HEPES (pH 7.9), 0.42 M NaCl, 1 mM EDTA, 1 mM EGTA; supplemented with 1x Halt™ protease and phosphatase inhibitor cocktail] for 30min on an orbital shaker at 600 U/min. Lysates were cleared by centrifugation for 30min at 4°C and 18,000 *g*. The supernatant was collected as the nuclear fraction and stored at -20°C. For SDS-PAGE, cytoplasmic and nuclear fractions were mixed with SDS-PAGE loading buffer. Nono/p54nrb and α-tubulin were used as controls for the nuclear and cytoplasmic fractions, respectively.

Protein extraction

For protein expression analysis, keratinocytes were lysed in SDS buffer [2.5% (v/v) SDS pH 7.5, 1 mM EDTA, 100 mM HEPES; supplemented with 1x Halt™ protease and phosphatase inhibitor cocktail (Thermo Fisher Scientific)] and centrifuged for 15min at 13,000 *g*. The protein concentration was determined using the Pierce™ BCA Protein Assay Kit (Thermo Fisher Scientific) according to the manufacturer's protocol. Benzonase (Santa Cruz Biotechnology, Dallas, Texas, USA) and SDS-PAGE loading buffer [250 mM Tris/HCl (pH 6.8), 30% (v/v) glycerol, 0.25% (w/v) bromophenol blue, 10% (v/v) β-mercaptoethanol, 8% (v/v) SDS] were added. Samples were heated to 95°C for 5min, separated by SDS-PAGE, and analyzed by western blotting.

RNA expression

Keratinocytes transfected in suspension with 2 pmol of the respective siRNA pools were maintained in LCM for 72h or switched to HCM at 48h after transfection and kept in HCM for another 24h. Cells were homogenized in Trizol and RNA isolated by phenol/chloroform extraction and isopropanol precipitation. For cDNA synthesis, 1 μg total RNA served as the template using SuperScript® II Reverse Transcriptase (Thermo Fisher Scientific) and random hexamer primers following the manufacturer's protocol. Real-time PCR was performed with primaQUANT 2x qPCR CYBR Green MasterMix w/o ROX (Steinbrenner-Laborsysteme GmbH, Wiesenbach, Germany) using a LightCycler 480 II Real Time PCR system (Roche, Basel, Switzerland) with the following PCR conditions: 95°C for 15min followed by 40 cycles of 95°C for 15 s, 62°C for 15 s, and 72°C for 20 s. Primer pairs were selected using Primer Blast (https://www.ncbi.nlm.nih.gov/tools/primer-blast/). The primer sequences are listed in Table S4.

SDS-PAGE and western blotting

Equal amounts of protein were separated by SDS-PAGE. Proteins were transferred to Amersham Protan™ nitrocellulose blotting membranes (pore size 0.2 μm, Th. Geyer, Renningen, Germany) using Mini Trans-Blot cells (Bio-Rad Laboratories, Hercules, California, USA). After transfer, membranes were stained in Ponceau S solution [0.2% (w/v) Ponceau S, 3% (w/v) TCA, 3% (w/v) sulfosalicylic acid] for 5min, washed in distilled water, and documented using a scanner. Membranes were cut, destained in Tris-buffered saline with Tween20 (TBST), blocked with 3% (w/v) skimmed milk/TBST or 3% (w/v) bovine serum albumin (BSA)/TBST, and subsequently probed overnight with the appropriate primary antibodies as listed in Table S2. Membranes were washed three times with TBST and incubated for 1h with the appropriate horseradish peroxidase-conjugated secondary antibodies (Dianova, Hamburg, Germany, see Table S3). Membranes were treated with ECL Western Blotting Substrate [equal parts chemiluminescence solution 1 (100 mM Tris/HCl [pH 8.5], 25 mM luminol, 0.4 mM coumaric acid) and 2 (100 mM Tris/HCl [pH 8.5], 0.02% [v/v] H_2O_2)] or Western Blot Ultra-Sensitive HRP Substrate (Takara) and chemiluminescence was detected using a Fusion-SL 3500WL imaging system (Peqlab, Erlangen, Germany). If staining with additional antibodies was required, the membranes were washed three times in TBST for 10min each, incubated in stripping buffer [0.2 M glycine, 0.05% tween-20 (pH 2.5)] for 1h, washed again in TBST (3× 10min), blocked, and treated with antibodies as described above. Glyceraldehyde-3-phosphate dehydrogenase (GAPDH) or Ponceau S staining was used as the loading control.

Gene set enrichment analysis

The Gene set enrichment analysis has been described previously.[19] Briefly, it was performed using the R-package clusterProfiler (v 4.8.2; and MSigDB mouse gene sets (v2023.1) utilizing the fgsea algorithm and setting the exponent parameter to 0 for unweighted analyses of log2 fold change sorted gene lists obtained from differential gene expression analyses.

QUANTIFICATION AND STATISTICAL ANALYSIS

Western blot quantification

For quantification of western blots, we used the ImageJ tool "Gel Analysis". All signals were normalized to the internal loading control GAPDH. If GAPDH expression varied due to experimental conditions, Ponceau S staining was used as the loading control. Details concerning normalization procedures are given in the figure legends.

Quantification of immunofluorescence

To determine the enrichment factors in the nucleus and cytoplasm, fluorescence intensities were measured as described previously.[59] Briefly, fluorescence intensities were measured in segments of equal length (100 pixels) and width (40 pixels) across individual nuclei. All nuclei of the entire image were evaluated with the exception of mitotic, polynuclear, or overgrowing cells. Each line scan resulted in a histogram depicting the fluorescence intensities along the bar. The enrichment factors for YAP and TAZ were calculated by dividing the mean nuclear value (50-pixel length at the start of the 100-pixel scan line) by the mean cytoplasmic value (50-pixel length at the end of the 100-pixel scan line) for each line scan. At least 100 cells were analyzed per condition from two independent experiments.

The quantification of fluorescence intensities at lateral contacts has been described previously.[60] Briefly, fluorescence intensities were measured in segments of equal length (about 100 pxl) and width (40 pxl) covering the cytoplasm as well as bicellular contacts. Each line scan results in a histogram depicting the fluorescence intensities along the bar. The enrichment factors for YAP and TAZ at bicellular contacts were calculated by dividing the mean junctional value (10 pxl length of the 100 pxl scan line) by the mean cytoplasmic value (both ends of a scan line, each 10 pxl length) for each line scan. At least 100 cells were analyzed per condition from two independent experiments.

Statistical analysis

Statistical analysis and plot preparation were performed using Graphpad Prism Software (version 8.3). All individual data points are shown in the plots. Boxplots display the first to third quartile; whiskers extend to the minimum and maximum. For two independent data sets, significant differences were determined by a two-tailed Student's t-test. To compare more than two independent data sets with normal distribution, one-way analysis of variance (ANOVA) followed by a Tukey's multiple comparison test was used.